

# Vascular wall microenvironment: Endothelial cells original exosomes mediated melatonin-suppressed vascular calcification and vascular ageing in a m<sup>6</sup>A methylation dependent manner

Su-Kang Shan<sup>a</sup>, Xiao Lin<sup>b</sup>, Feng Wu<sup>c</sup>, Chang-Chun Li<sup>a</sup>, Bei Guo<sup>a</sup>, Fu-Xing-Zi Li<sup>a</sup>, Ming-Hui Zheng<sup>a</sup>, Yi Wang<sup>a</sup>, Qiu-Shuang Xu<sup>a</sup>, Li-Min Lei<sup>a</sup>, Ke-Xin Tang<sup>a</sup>, Yun-Yun Wu<sup>a</sup>, Jia-Yue Duan<sup>a</sup>, Ye-Chi Cao<sup>a</sup>, Yan-Lin Wu<sup>a</sup>, Chang-Ming Tan<sup>d</sup>, Zi-Han Liu<sup>d</sup>, Zhi-Ang Zhou<sup>d</sup>, Xiao-Bo Liao<sup>d</sup>, Feng Xu<sup>a,\*\*</sup>, Ling-Qing Yuan<sup>a,\*</sup>

<sup>a</sup> National Clinical Research Center for Metabolic Diseases, Department of Metabolism and Endocrinology, The Second Xiangya Hospital of Central South University, Changsha, 410011, Hunan, People's Republic of China

<sup>b</sup> Department of Radiology, The Second Xiangya Hospital of Central South University, Changsha, Hunan Province, 410011, People's Republic of China

<sup>c</sup> Department of Pathology, The Second Xiangya Hospital of Central South University, Changsha, 410011, People's Republic of China

<sup>d</sup> Department of Cardiothoracic Surgery, The Second Xiangya Hospital of Central South University, Changsha, 410011, People's Republic of China

## ARTICLE INFO

### Keywords:

Melatonin  
Vascular calcification  
Vascular ageing  
Exosomes  
N<sup>6</sup>-methyladenosine

## ABSTRACT

Vascular calcification and vascular ageing are “silent” diseases but are highly prevalent in patients with end stage renal failure and type 2 diabetes, as well as in the ageing population. Melatonin (MT) has been shown to induce cardiovascular protection effects. However, the role of MT on vascular calcification and ageing has not been well-identified. In this study, the aortic transcriptional landscape revealed clues for MT related cell-to-cell communication between endothelial cells (ECs) and vascular smooth muscle cells (VSMCs) in vascular calcification and vascular ageing. Furthermore, we elucidated that it was exosomes that participate in the information transportation from ECs to VSMCs. The exosomes secreted from melatonin-treated ECs (MT-ECs-Exos) inhibited calcification and senescence of VSMCs. Mechanistically, miR-302d-5p was highly enriched in MT-ECs-Exos, while depletion of miR-302d-5p blocked the ability of MT-ECs-Exos to suppress VSMC calcification and senescence. Notably, Wnt3 was a bona fide target of miR-302d-5p and modulated VSMC calcification and senescence. Furthermore, we found that maturation of endothelial derived exosomal miR-302d-5p was promoted by WTAP in an N<sup>6</sup>-methyladenosine (m<sup>6</sup>A)-dependent manner. Interestingly, MT alleviated vascular calcification and ageing in 5/6-nephrectomy (5/6 NTP) mice, a chronic kidney disease (CKD) induced vascular calcification and vascular ageing mouse model. MT-ECs-Exos was absorbed by VSMCs in vivo and effectively prevented vascular calcification and ageing in 5/6 NTP mice. ECs-derived miR-302d-5p mediated MT induced anti-calcification and anti-ageing effects in 5/6 NTP mice. Our study suggests that MT-ECs-Exos alleviate vascular calcification and ageing through the miR-302d-5p/Wnt3 signaling pathway, dependent on m<sup>6</sup>A methylation.

## 1. Introduction

Vascular calcification often co-exist with the development of advanced atherosclerosis [1]. Emerging evidence has revealed higher

morbidity and mortality of cardiovascular events in patients with vascular calcification [2]. After decades of intensive research, vascular calcification, a unique phenotype of vascular ageing, has now been demonstrated to be an active and systematically regulated biological

Peer review under responsibility of KeAi Communications Co., Ltd.

\* Corresponding author. National Clinical Research Center for Metabolic Diseases, Department of Metabolism and Endocrinology, The Second Xiangya Hospital of Central South University, Changsha, 410011, Hunan, People's Republic of China.

\*\* Corresponding author. National Clinical Research Center for Metabolic Diseases, Department of Metabolism and Endocrinology, The Second Xiangya Hospital of Central South University, Changsha, 410011, Hunan, People's Republic of China.

E-mail addresses: [feng.xu@csu.edu.cn](mailto:feng.xu@csu.edu.cn) (F. Xu), [allenylq@csu.edu.cn](mailto:allenylq@csu.edu.cn) (L.-Q. Yuan).

<https://doi.org/10.1016/j.bioactmat.2024.08.021>

Received 28 January 2024; Received in revised form 10 August 2024; Accepted 20 August 2024

2452-199X/© 2024 The Authors. Publishing services by Elsevier B.V. on behalf of KeAi Communications Co. Ltd. This is an open access article under the CC BY-NC-ND license (<http://creativecommons.org/licenses/by-nc-nd/4.0/>).

process. It has been progressively recognized that vascular function depends on the bidirectional interactions between vascular cells and their microenvironment [3]. Most studies, if not all, have proposed that phenotypic switch of contractile vascular smooth muscle cells (VSMCs) into secreting osteoblast-like VSMCs contributes to vascular calcification [4–6]. Notably, the phenotypic transition of VSMCs is subtly modulated by various factors, including adipokines and non-coding RNAs [7–9]. However, the roles of the vascular wall microenvironment in the progression of vascular calcification and vascular ageing remain largely unknown.

Melatonin (MT) is a classical indole neuroendocrine hormone that plays a vital role in maintaining normal sleep rhythms and metabolic homeostasis. Indeed, MT induced cardio-protection effects by reducing myocardial injury, alleviating cardiomyopathy, and enhancing endothelial function [10,11]. Our previous study showed that MT attenuated vascular calcification by targeting VSMCs in a paracrine-dependent manner. However, in the vascular microenvironment, the MT-induced cell-cell communication remains to be elucidated.

Accumulating insight has been driven into exosomes, a well-known subtype of extracellular vesicles with a diameter between 40 and 150 nm, which have the capability to package proteins, lipids, and nucleic acids including miRNAs and then transfer into the recipient cells to exhibit profound biological effects [12]. Exosomes have now emerged as crucial components that mediate intercellular communication and tissue crosstalk in the cardiovascular system [13,14]. Moreover, exosomes serve as a rising star of therapeutic targets for drug delivery and diagnosis markers [15–18]. Importantly, endothelial cells (ECs) derived exosomes containing proteins were capable of modulating VSMC proteomes and altering vascular inflammation [19]. Interestingly, VSMCs-derived exosomes containing miR-155 transferred to endothelial cells and enhanced endothelial permeability, resulting in atherosclerotic progression [20]. Recently, we have also revealed that exosomes derived from VSMCs alleviate vascular calcification by affecting nearby VSMCs in a paracrine manner [21]. Therefore, only partial exosomal components have been identified and the specific aortic cell-derived exosomes involved in MT's anti-calcification and anti-ageing effect remain to be elucidated.

## 2. Materials and methods

### 2.1. Ethics statement

All the surgical experiment procedures and animal feeding protocols conform to Guide for the Care and Use of Laboratory Animals, NIH publication, 8th edition, 2011. All the human studies were in compliance with the principles of the Declaration of Helsinki and written informed consent was obtained by all the participants before the studies. All the animal and human studies were approved by the Ethics Committee of the Second Xiangya Hospital, Central South University. VSMCs were obtained and authenticated by a previously established method [21]. Primary Aortic ECs were purchased from American Type Culture Collection (ATCC) and authenticated by Short tandem repeat (STR) profiling.

### 2.2. Reagents

The fetal bovine serum (FBS), DMEM and penicillin/streptomycin solutions were purchased from Gibco-BRL Co., Ltd (Grand Island, NY, USA). MT (M5250),  $\beta$ -glycerophosphate ( $\beta$ -GP) (50020), GW4869 (D1692), PKH26 Red Fluorescent Cell Linker Kit (PKH26PCL), Alizarin Red S (A5533), silver nitrate (S8157) and Senescence Cells Histochemical Staining Kit (CS0030) were bought from Sigma-Aldrich (St Louis, MO, USA). DMEM/F12 (12634010) and Fetal bovine serum (10099133C) were purchased from Gibco BRL Co. (Grand Island, NY, USA). Lipofectamine 2000 (11668019) was purchased from Invitrogen Co. (Carlsbad, CA, USA). Antibodies for GAPDH and Horseradish

Peroxidase (HRP)-conjugated Goat Anti-Mouse IgG, m6A Monoclonal antibody(68055-1-Ig,1:2000) as well as HRP-conjugated Goat Anti-Rabbit IgG were purchased from Proteintech (Rosemont, USA). Antibodies for P21 (ab218311, 1:1500), CD63 (ab134045, 1:5000), CD81 (ab59477, 1:1000), Grp94 (ab3674, 1:2000), Wnt3 (ab32249, 1:1000) and Runx2 (ab23981, 1:1000) were purchased from Abcam (Cambridge, UK). Maxima SYBR Green/ROX qPCR Master Mix (C0210B) and all primers used in this study were purchased from GeneCopoeia (Rockville, MD, USA). The ECL detection kit (sc-2048) was purchased from Santa Cruz Biotechnology, Inc. (Santa Cruz, CA, USA). Wnt3 small interfering RNA (siRNA) oligos, WTAP small interfering RNA, HNRNPA2B1 and control siRNA oligos were purchased from RiboBio (Guangzhou, China). FAM-labeled-miR-302d-5p mimics (miR1200707041413), FAM-labeled-inhibitors (miR2200707041519), FAM-labeled miR-126-3p mimics and their control oligonucleotides were purchased from RiboBio (Guangzhou, China). DAPI (C0065) was purchased from Solarbia (Beijing, China). AAV9-TIE-miR-302-eGFP or control were designed and synthesized by Shanghai GeneChem Co., Ltd. (Shanghai, China).

### 2.3. Bioinformatics analysis of single-cell RNA-seq

Dimensional reduction, clustering, and analysis of single-cell RNA sequencing data were performed using the R package Seurat (Version 2.3.1). We used the MergeSeurat function to merged the data sets. Cells with expression of fewer than 200 or more than 4000 genes and cells with greater than 20 % expression of mitochondrial genes were filtered out of the analysis. The filtered data were standardized by “Normalize Data” and preprocessed by the “FindMarkers” in the Seurat software to identify variation genes in different samples.

The top 2000 variable genes were selected by FindVariableFeatures for PCA analysis. Uniform Manifold Approximation and Projection (UMAP) was performed using Seurat functions based on PCs 1–20, and clustering to define cell identity was performed using the Seurat FindClusters function with resolution = 1. Marker genes for each cluster were determined using the Wilcoxon rank-sum test via the FindAllMarkers function in Seurat by  $\log_2FC > 0.25$  and  $\text{min.pct} = 0.1$ . Gene Ontology (GO) and Kyoto Encyclopedia of Genes and Genomes (KEGG) analyses were used with the “clusterProfiler” R package version 3.5.1. Pathways with adjusted  $p$  value less than 0.05 were considered as significantly enriched. The relationship between potential ligand and receptor interactions were quantified by CellPhoneDB using python package. The results were visualized using dot plots and heatmaps.

### 2.4. Cell culture and transfection

Human VSMCs were obtained and authenticated using a previously established method [22]. VSMCs and ECs were maintained in a medium containing DMEM, 10 % exosome-free FBS, and 1 % penicillin/streptomycin (15070063, Gibco). All cells were incubated at 37 °C with a humidified atmosphere containing 5 % CO<sub>2</sub>. Free of mycoplasma infection in VSMCs was confirmed by mycoplasma testing kit (Shanghai Seo Biotechnology Co., Ltd). VSMCs passaged for 4 to 6 times were chosen for the cell experiments and a medium containing 10 mM  $\beta$ -GP was used to induce VSMCs calcification as reported previously [23]. To induce senescence of VSMCs, cells were starved at 0.1 % FBS medium overnight to achieve synchronization and then Ang II (0.3  $\mu$ M, #A6778, Sigma) was added and cultured for 5 days. Cells at 50 % confluency were transfected with miR-302-5p mimics (50 nM), inhibitor (100 nM), Wnt3 siRNA (50 nM), or Dicer siRNA (50 nM), WTAP siRNA (50 nM), HNRNPA2B1 siRNA (50 nM) by using HiperFect Transfection Reagent (301704, Qigen, Hilden, Germany) according to the manufacturer's instructions.

### 2.5. Co-culture and fluorescent tracing

ECs and VSMCs were co-cultured using with 0.4  $\mu$ m transwell inserts

(3412, Corning, USA). ECs, pretreated with or without GW4869 (Sigma, USA), were transfected with 5'FAM fluorescently labeled miR-302d-5p mimic (Ruibo, china), then transferred to inserts, and placed in the upper chamber of a six-well plate where VSMCs were cultured, after co-cultured for 48 h, the upper chamber was removed, and the culture medium of VSMCs was discarded, VSMCs were then washed in PBS and fixing with 4 % paraformaldehyde for 15 min, subsequently permeabilized with 0.4 % TritonX-100 solution for 10 min. The cells were then washed with PBS solution and incubated with 1 mL of diluted YF®594-Phalloidin dye (UElandy, china) for 20 min, followed by staining with DAPI for 3 min. Finally, images were obtained using a laser confocal microscope (BC43, Andor Technology, UK).

## 2.6. Exosomes purification and characterization

Ultracentrifugation was performed to isolate exosomes from the supernatants of ECs cultures. ECs were incubated with DMEM with exosome-free serum and then subjected to MT or vehicle control. The cultured medium was centrifuged at  $2000 \times g$  for 15 min at  $4^\circ\text{C}$ , followed by a second centrifugation at  $12,000 \times g$  for 45 min at  $4^\circ\text{C}$  to remove dead cells and platelets. The resulting supernatants were filtered through a 0.22- $\mu\text{m}$  filter (Millipore) and ultracentrifuged at  $100,000 \times g$  for 2 h at  $4^\circ\text{C}$ . The resulting pellets were washed with PBS followed by a secondary ultracentrifugation at  $100,000 \times g$  for 2 h at  $4^\circ\text{C}$ , and resuspended in PBS. The isolated exosomes were subjected to transmission electron microscopy (Hitachi H-7650, Hitachi, Tokyo, Japan) for morphology analysis, and Nanosight 2000 (Particle Metrix, Germany) for diameter analysis. Exosomes were further identified by Western blot by exosomal marker proteins (CD63, CD81, and TSG101) by Western blot. The PKH26 Red Fluorescent Cell Linker kit (sigma, USA) was used to label exosomes to monitor tracking, according to the manufacturer's instructions.

## 2.7. Quantitative reverse transcription-polymerase chain reaction (qRT-PCR)

Total RNA from exosomes and the cells was extracted using TRIzol reagent (Invitrogen, Carlsbad, CA, USA) according to the manufacturer's instructions. For miRNAs expression detection, miRNA was reverse transcribed and subjected to qRT-PCR using the All-in-One™ miRNA quantitative RT-PCR Detection System (GeneCopoeia, Rockville, USA) following the manufacturer's protocol. Using U6 (for cellular miRNAs), or miR-16 (for exosomal miRNAs) as the normalized control. miRNAs and U6 primers were purchased from GeneCopoeia.

## 2.8. Western blot analysis

Proteins analysis by Western blot was performed as described previously [24]. Briefly, total proteins were isolated using RIPA buffer lysate (Beyotime Biotechnology, Shanghai, China) supplemented with a cocktail protease inhibitor (Selleck, Shanghai, China). Equal amounts of protein (30  $\mu\text{g}$ ) were subjected to Western blot and the reaction was determined with Luminata™ Crescendo Western HRP Substrate (Millipore, Billerica, MA). Bands were visualized and analyzed using ABI system.

## 2.9. Analysis of the ALP activity

The cellular lysates solution was scraped from cells and then subjected to the p-nitrophenol release reaction at  $37^\circ\text{C}$ . The ALP activity was measured by detecting p-nitrophenol release using the ALP kit (Jiancheng Nanjing Biological Engineering, Nanjing, China), as previously reported [25].

## 2.10. Alizarin Red S staining and calcium content

Alizarin Red S staining was performed in the same way as described previously [21]. Briefly, cells or artery tissues were fixed in 4 % formaldehyde and then subjected to Alizarin Red S solution (2 %, wt/vol, pH 4.2) for 3 min following by wash three times with PBS to reduce nonspecific staining. The stained matrix was digitally photographed. To determine calcium content, cells with calcifying nodules were incubated with HCl and then analyzed using the o-cresolphthalein method. The resulting solution was measured by atomic absorption spectroscopy.

## 2.11. SA- $\beta$ -gal staining assay

SA- $\beta$ -gal staining was performed using a SA- $\beta$ -gal staining kit (Sigma-Aldrich, St Louis, MO, USA) as reported previously according to the manufacturer's instructions [21]. Briefly, cells or aorta samples were fixed in a solution containing 2 % formaldehyde and 0.2 % glutaraldehyde, followed by incubation with SA- $\beta$ -gal staining solution (pH = 6.0) for 18 h at  $37^\circ\text{C}$ . Random images were selected to calculate the percentage of SA- $\beta$ -gal-positive cells or area.

## 2.12. Luciferase reporter gene assay system

The fragment of the wild type Wnt3 3'-UTR, containing potential binding sites of miR-302d-5p seed regions, or mutant Wnt3 3'-UTR (mutants at the miR-302d-5p seed regions) was ligated into a pmirGLO-dual-luciferase miRNA target expression vector (Promega, USA) in a similar way as reported previously [23]. The constructed vectors were then identified by sequencing, cloned, and purified. VSMCs were co-transfected with a luciferase reporter carrying wild-type Wnt3 3'-UTR or mutant Wnt3 3'-UTR, and miR-302d-5p mimics or scramble oligonucleotides. Subsequently, luciferase activities were analyzed using the luciferase assay system (Promega) after 48 h transfection. The nucleotide sequences of primers used in the construction and mutation of Wnt3 3'-UTR mRNA were purchased from Ribobio.

## 2.13. RNA m6A quantification

The total RNA in ECs was extracted, diluted to different concentrations, the continuously diluted mRNA was denatured at a high temperature of  $95^\circ\text{C}$ , and rapidly cooled. Then, 2  $\mu\text{L}$  of mRNA was transferred directly to a nylon membrane for ultraviolet cross-linking, and the unbound mRNA was washed off in a gentle manner and incubated with 5 % BSA for 1 h at room temperature. The membrane was then incubated with 10 mL of anti-m6A antibody dilution buffer under gentle shaking conditions at  $4^\circ\text{C}$ . After washing the membrane, the membrane was washed and the nylon membrane was incubated with sheep anti-mouse IgG-HRP at room temperature, followed by ECL development for observation. The m6A content was also measured by ELISA using an EpiQuik m6A RNA methylation quantification kit (Epigentek) following the manufacturer's instruction. Briefly, 200 ng RNA was added to the wells of the assay plate. Subsequently, the capture antibody solution and the detection antibody solution were added to the assay wells. The m6A levels were quantified with colorimetry method by reading the absorbance of each well at 450 nm, and relative m6A abundance was calculated according to manual.

## 2.14. RNA immunoprecipitation (RIP) assay

ECs with downregulated WTAP expression were lysed with RIP lysis buffer (absin) at  $4^\circ\text{C}$  through disruptive sonication. Immunoprecipitation of endogenous DGCR8 was performed using an anti-DGCR8 antibody (Abcam) or control IgG antibody overnight at  $4^\circ\text{C}$ . After washing, the immunoprecipitated protein-RNA complex was treated with proteinase K. RNAs were extracted using standard phenol/chloroform procedure. Then, the pri-miRNAs were detected with qRT-PCR, and %

(IP/Input) and % (IgG/Input) were obtained. Finally, the relative m6A level on pri-miRNAs was calculated by  $\%(\text{IP}/\text{Input})/\%(\text{IgG}/\text{Input})$ . For m6A RIP (MeRIP) experiments, RNA extracted from ECs with down-regulated WTAP and control ECs was treated with deoxyribonuclease I (Sigma). The RNAs were fragmented by sonication for 10s on the ice-water mixture. Immunoprecipitation was performed using an anti-m6A antibody (proteintech) or control IgG antibody previously bound to magnetic beads (Bimake) in the RIP immunoprecipitation buffer (Millipore) and incubated with DNA-free fragmented RNAs. Beads were then treated with proteinase K (20 mg/mL) for 1.5 h at 42 °C. RNAs were extracted by standard phenol/chloroform procedure. Then, the pri-miRNAs were detected with qRT-PCR, and  $\%(\text{IP}/\text{Input})$  and  $\%(\text{IgG}/\text{Input})$  were obtained. The relative level of pri-miRNAs binding to DGCR8 was calculated by  $\%(\text{IP}/\text{Input})/\%(\text{IgG}/\text{Input})$ .

### 2.15. Construction of nephrectomy induced chronic kidney disease (CKD) mice model

Male C57BL/6 mice (six-week of age) were purchased from Hunan SJA Laboratory Animal Co., LTD (Hunan, China) and housed with 12-h daylight/darkness transition in Animal House of the Second Xiangya Hospital. The 5/6 NTP mice calcification model was established following the procedure described previously [26]. The endothelial specific overexpression of miR-302d-5p in mice artery was achieved by injecting AAV9-TIE-miR-302-eGFP into the aorta segment [27]. If necessary, MT was administered via gavage (i.g.) at the concentration of 20 mg/kg daily [28]. Exosomes (200 µg/d) were administered to mice via tail vein injections at three-days intervals for four weeks. Aortic tissues were carefully harvested for further analysis.

### 2.16. In vivo tracking of exosomes and exosomes injection

To track the distribution of exosomes in vivo, 1,1'-Diiodo-3,3',3'-Tetramethylindotricarbocyanine Iodide (DiI, 2024243, Thermo Fisher Scientific/Invitrogen, Waltham, USA) was used to label the exosomes. DiI or DiR labeled exosomes were injected via the tail vein, and in vivo fluorescence images were taken 0, 4, 8, 12, 24 h using Ami X spectral imaging instrument and quantified using in vivo imaging software.

### 2.17. Immunohistochemistry

Thoracic aorta tissues were fixed in 4 % paraformaldehyde following by paraffin-embedded process [29]. Subsequently, sections were dewaxed in xylenes and then dehydrated in 99 %, 95 %, and 75 % ethanol. Endogenous peroxidases were quenched by hydrogen peroxide incubation, and antigen retrieval was performed using citrate incubation. Sections were then blocked by 5 % fetal serum, following by incubating with antibodies against Runx2 and P21 overnight at 4 °C with gentle rocking. After incubation with a secondary antibody, positive staining was detected by the DAB kit (GK5007, GTvision, Shanghai, China). Random selected photographs were analyzed using Image-pro Plus software (version 6.0).

### 2.18. Vascular immunofluorescence

To identify CD81 level in the thoracic aorta, mouse aorta tissues were isolated on ice following by mounting in OCT-embedded process. To induce double color staining, frozen aortic sections were sequentially incubated with monoclonal antibody against exosomal marker CD81 (ab59477, 1:100) and VSMCs marker  $\alpha$ -SMA (GB13044, 1:500) followed by incubation with Cy3-conjugated Goat Anti-rabbit IgG (GB21303, 1:300) and Alexa Fluor®488-conjugated Goat Anti-mouse IgG (GB25301, 1:400). Positive staining was assessed using a fluorescence confocal microscope (Nikon).

### 2.19. Statistical analysis

SPSS 23.0 (SPSS, Chicago, IL, USA) was used for all statistical comparisons. Data are presented as mean  $\pm$  standard error of the mean (SEM.), with 'n' indicating the number of independent experiments conducted. Normality of data distribution was confirmed using the Kolmogorov-Smirnov test. Differences between groups were assessed using parametric tests (two-tailed Student's t-test for two groups, one-way ANOVA for multiple groups) under assumptions of normality and homogeneity of variances. Non-parametric tests (Mann-Whitney U test for two independent groups, Kruskal-Wallis test for multiple groups) were employed where data did not meet parametric assumptions. Post hoc comparisons utilized Dunnett's or Tukey's tests for parametric data and appropriate non-parametric equivalents. Statistical significance was defined as  $p < 0.05$ .

## 3. Results

### 3.1. Single-cell RNA-seq revealed altered endothelial MT activity along with predominant ECs-VSMCs communication in patients with CVD

Vascular calcification and ageing are prevalent and pathological basis for cardiovascular diseases (CVD) [30]. In an attempt to investigate the potentially relevant cell types associated with vascular calcification and ageing in the vascular wall, we integrated and reanalyzed the single-nucleus RNA sequencing (snRNA-seq) datasets of aorta in previous researches involving common transcriptional landscape from patients with CVD and their controls [31,32] (Fig. 1A). Through comparison of unique transcriptional profiles in each cluster to canonical cell markers, nine primary cell clusters were identified, comprising VSMCs, fibroblasts, ECs, adipocyte, neuronal, lymphatic ECs (LECs), pericyte, as well as macrophages and lymphocytes (Fig. 1B). Of note, LECs were functionally and anatomically distinct from blood vascular ECs (referred to "ECs"), and the identification of neuronal cell validate the existence of neuroimmune cardiovascular interfaces during atherosclerosis pathogenesis [33]. Heatmap analysis of the top-10-ranking markers revealed distinct signatures of cells in the vascular wall (Supplemental Figure Ia). Interestingly, there was significant heterogeneity in cell distribution between patients and healthy controls (Supplemental Figure Ib), but the difference was not statistically significant (Supplemental Figure Ic). Importantly, we analyzed the cell-specific expression of MT receptors of aorta from single cell RNA sequence. We found that the receptors of MT, mainly type 1 (MTNR1A), downregulated significantly in patients with CVD, especially in ECs (Fig. 1C). Meanwhile, the expression of MTNR1A was confirmed to down-regulated in CKD induced vascular calcification mice compared with normal mice (Supplemental Figure II), confirming impaired MT signaling in ECs under CVD status. Moreover, we determined the cell-specific expression of genes with known coding mutations associated with vascular calcification [34]. The plurality of the genes showed highest expression in ECs and VSMCs, confirming their predominant roles in the pathogenesis of vascular disease (Fig. 1D). Results of cellular communication suggested that the intensity of ligands, receptors and their interactions in ECs-VSMCs increased in patients with CVD compared with healthy control (Fig. 1E), indicating the critical role of ECs-VSMCs communication under CVD status. GSEA analysis of the top-50-ranking expressed gene sets revealed that the differentially expressed gene sets involved in different biological processes (Fig. 1F). Indeed, highly expressed gene sets involved in blood vessel remodeling included VSMCs, ECs, fibroblast, macrophage and adipocyte, corresponding with our previous researches [3,19–21]. And the ECs contribute to regulation of response to drug, in agreement with the immediate reaction with exogenous MT. These data indicate dysfunctional endothelial MT activity along with critical ECs-VSMCs communication in patients with CVD.

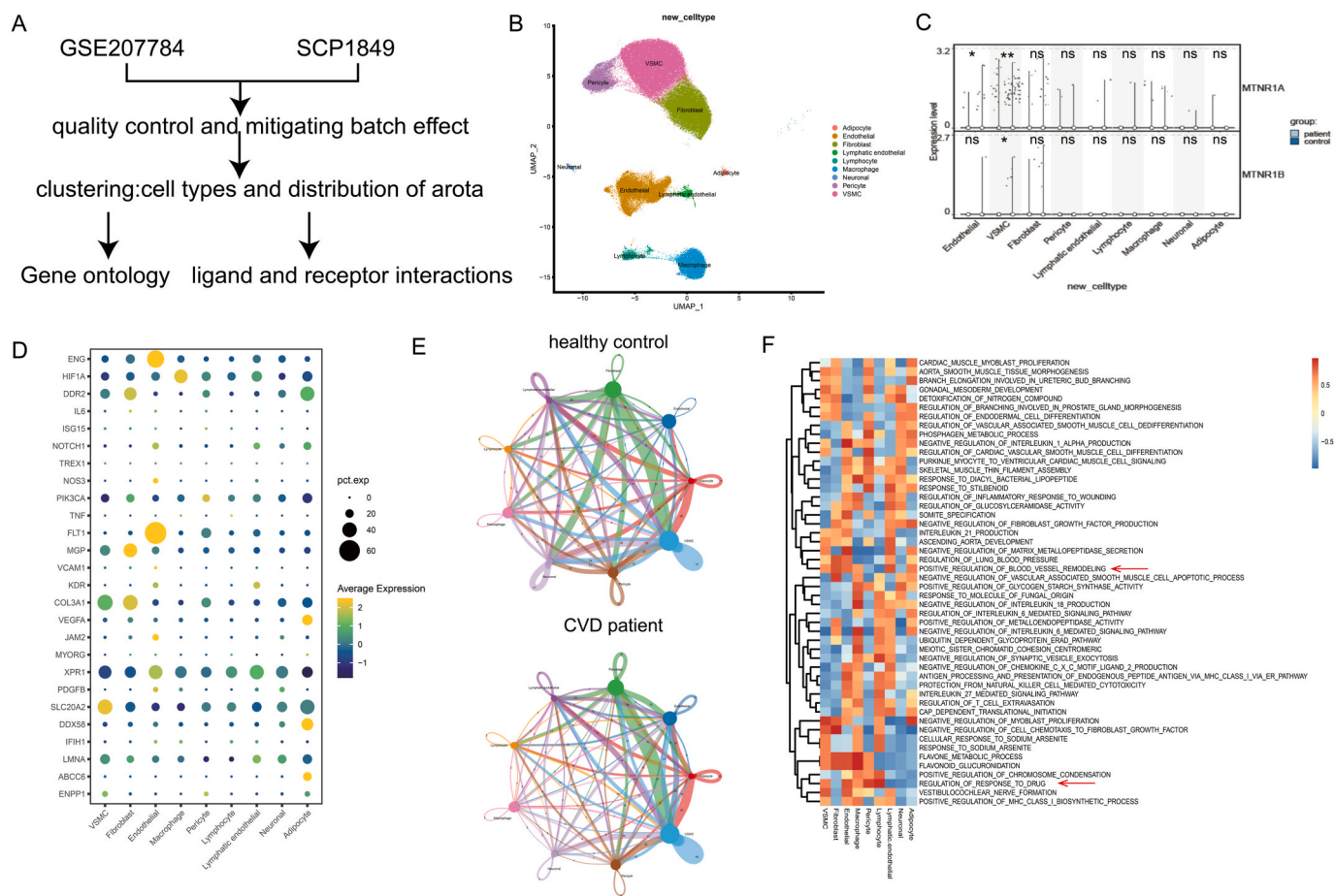


**Fig. 1.** Single-Cell RNA-Seq revealed aortic transcriptional landscape and melatonin related EC-VSMC communication in CVD and healthy controls. (A) Schematic diagram of the experimental design. (B) Uniform Manifold Approximation and Projection (UMAP) representation of aligned gene expression data in single cells extracted from control ( $n = 15$ ) and CVD ( $n = 13$ ) aortas. (C) Violin plots for gene expression of melatonin receptors in cell populations of aorta from patients with CVD and controls. (D) Cell-specific expression of genes with known coding mutations associated with CVD. (E) Cell-Cell communication analysis of cells between CVD patients and control volunteers by cellphone DB. (F) GO analysis of top 50 differentially expressed genes in patients with CVD and controls (ordered by decreasing  $p$  value).

### 3.2. Exosomes transferred from ECs to VSMCs

To investigate whether ECs could communicate with VSMCs in vascular microenvironment, ECs were transfected with FAM-labeled miR-126-3p mimics, a ECs specific expressed miRNA [35], then co-cultured with VSMCs by using transwell system (Fig. 2A). Notably, green fluorescence was appeared in VSMCs in the lower chamber, indicating that FAM-labeled miR-126-3p was delivered from ECs to VSMCs (Fig. 2B). Moreover, the expression of miR-126-3p in VSMCs increased after co-culturing with ECs transfected with FAM-labeled miR-126-3p compared with those co-culturing with ECs transfected with control dye (Fig. 2C). To determine whether exosomes mediate crosstalk between ECs and VSMCs. We isolated exosomes from ECs, as demonstrated by nanoparticle tracking analysis and electronic transmission microscope with a diameter between 50 and 140 nm (Fig. 2D and E). Moreover, these particles were abundant of exosomes specific markers CD9, CD81, and TSG101, while endoplasmic reticulum protein marker Grp94 was absent (Fig. 2F). These data indicated that we successfully isolated exosomes from the culture medium. Interestingly, by quantitative analysis of the expression level of EVs hallmarks from the snRNA sequencing data, there was no significant difference between CVD patients and healthy control (Supplemental Figure III a). While there was an increase in the number of particles (Supplemental Figure III b), protein content (Supplemental Figure III c), and expression of exosomal marker CD9 (Supplemental Figure III d) produced per milliliter of

supernatant. Altogether, the results confirmed that MT significantly promoted the secretion of ECs-derived exosomes. To further examine whether exosomes could be absorbed by VSMCs, we labeled ECs-derived exosomes with PKH26 and incubated VSMCs with these exosomes. Remarkable red fluorescence marked ECs-derived exosomes were observed in VSMCs (Fig. 2G), indicating sufficient absorption of ECs-exosomes by VSMCs. Interestingly, prior treatment of ECs with GW4869, an exosome secretion inhibitor, abrogated green fluorescence staining in recipient VSMCs that co-cultured with FAM-miR-126-3p labeled ECs (Fig. 2H). Taken together, exosomes containing miRNAs transferred from ECs to VSMCs, which might mediate crosstalk between these cells in the microenvironment of vascular wall.

### 3.3. Exosomes derived from MT-treated ECs mediated the anti-calcification and anti-senescence effects of melatonin in vitro

Previous studies have revealed that exosomes derived from ECs drive the physiological and pathological processes of VSMCs [23,24]. More recently, our research found that exosomes derived from MT-treated VSMCs induced inhibitory effects on vascular calcification and vascular ageing [21]. To determine whether melatonin antagonizes VSMCs calcification and senescence by inducing secretion of exosomes, VSMCs calcification was induced by  $\beta$ -GP (10 mM), while senescence was induced by 0.1 % FBS starvation and Ang II (0.3  $\mu$ M). Subsequently, VSMCs were incubated with culture medium (CM) collected from ECs,

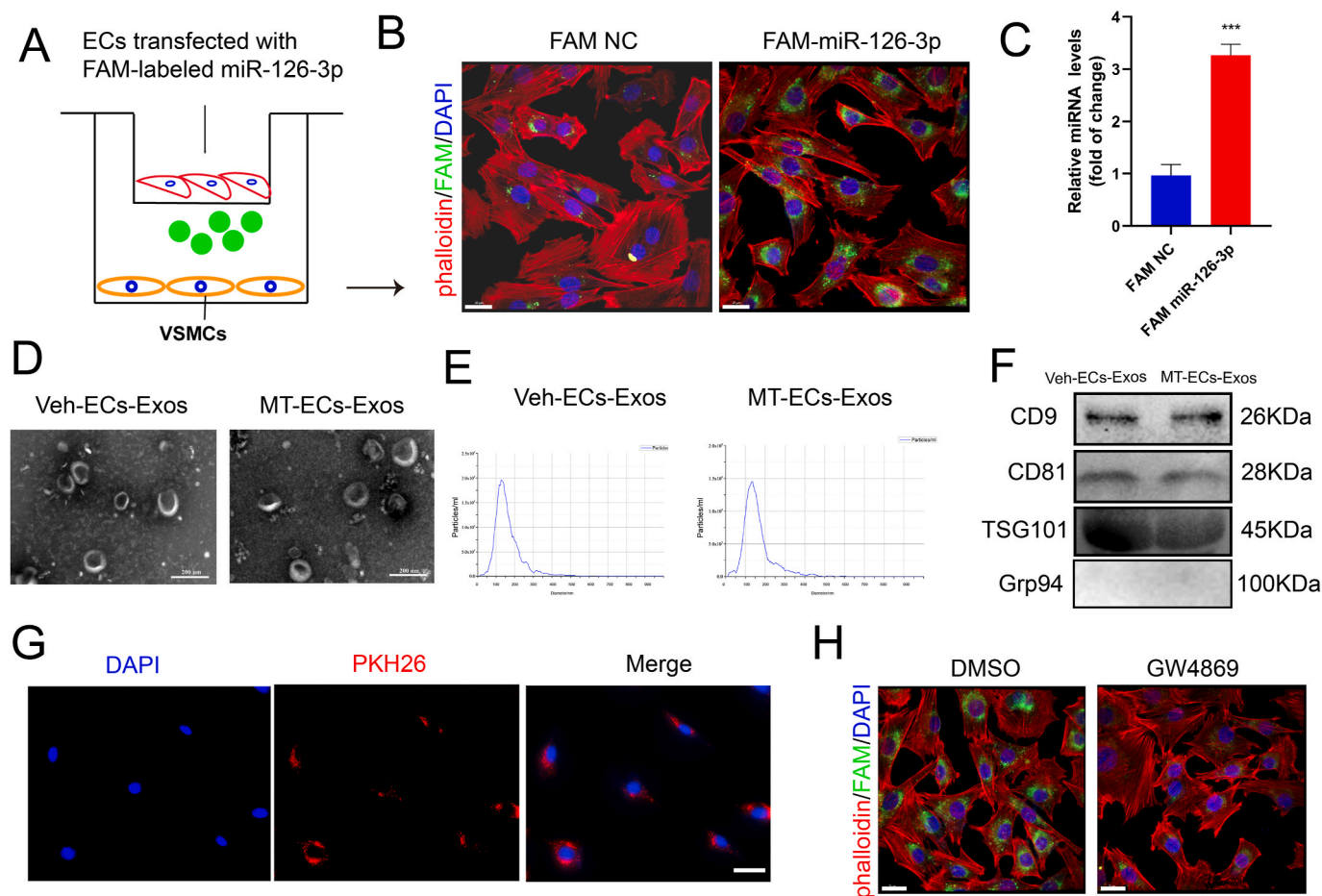


**Fig. 2.** Exosomes transferred from ECs to VSMCs. (A) Schematic diagram of transwell co-culture system. VSMCs were co-cultured with ECs transfected with FAM-labeled miR-126-3p or FAM alone. (B) Fluorescence signal detection in VSMCs within co-culture system by confocal microscope (scale bar = 20  $\mu$ m). (C) The expression level of miR-126-3p in co-cultured VSMCs by qRT-PCR. (D) Morphologic detection of exosomes by laser electron microscope (scale bar = 200 nm). (E) Particle diameter and concentration of exosomes detected by Malvern's NanoSight NS300. (F) The protein expression level of CD9, CD81, TSG101 and Grp94 detected by Western blot. (G) VSMCs were treated with PKH26 (red) labeled exosomes, and the fluorescence signal was detected by inverted fluorescence microscope (scale bar = 100  $\mu$ m). (H) VSMCs co-cultured with ECs treated with DMSO or GW4869 prior to transfection with FAM labeled miR-126-3p or FAM alone. Fluorescence signal detection in VSMCs by confocal microscope (scale bar = 20  $\mu$ m). Three independent experiments were performed, and representative images were shown. Data were shown as mean  $\pm$  SEM. \*\*\* $p$  < 0.001.

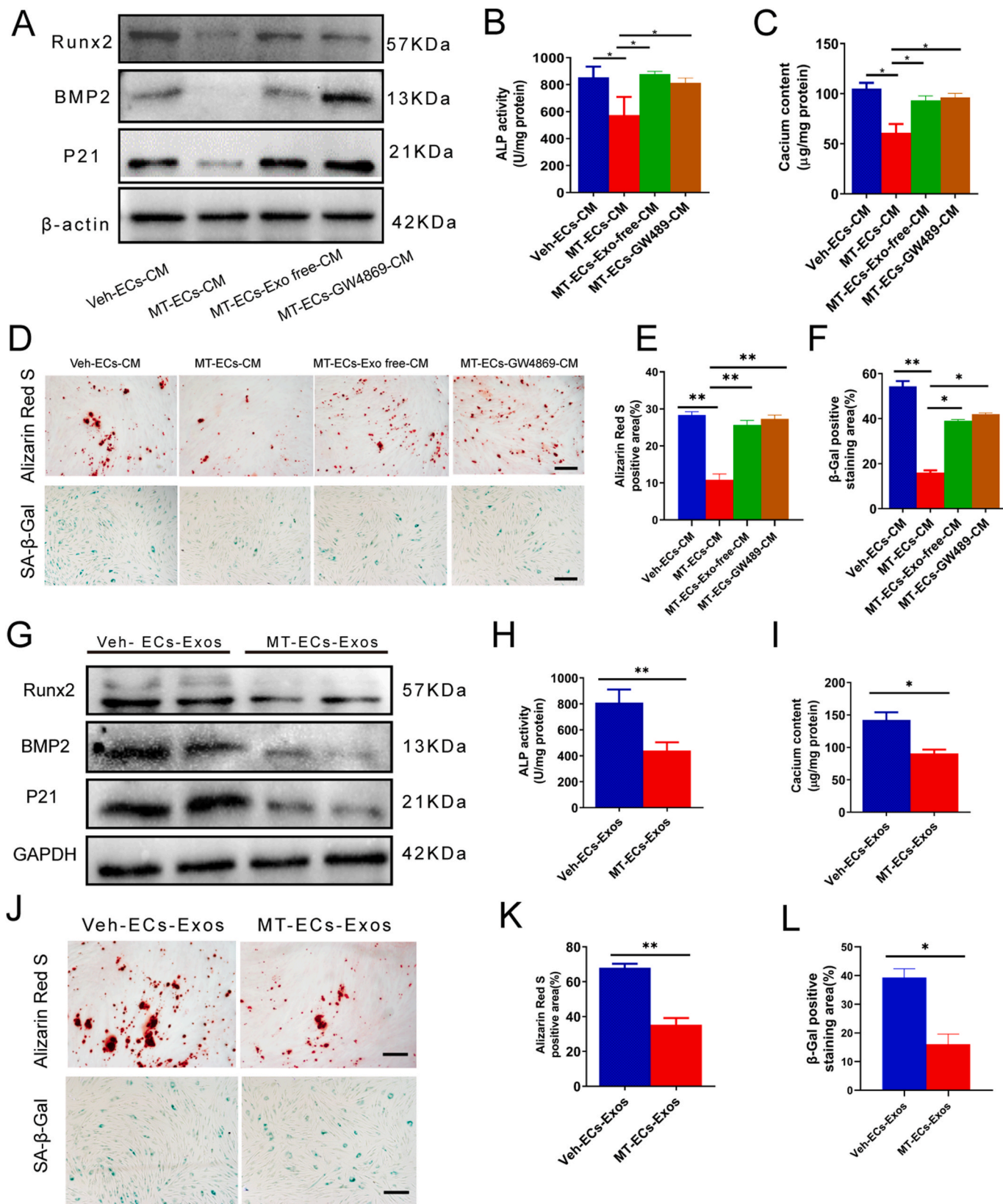
including vehicle-treated CM (Veh-ECs-CM), MT-treated CM (MT-ECs-CM), MT-ECs-CM with depletion of exosomes by differential centrifugation (MT-ECs-Exo-free-CM), or MT-ECs-CM with inhibition of exosomes secretion by GW4869 (MT-ECs-GW4869-CM). The Results demonstrated that MT-ECs-CM decreased Runx2, BMP2 expression (Fig. 3A), ALP activity (Fig. 3B), calcium content (Fig. 3C) and level of Alizarin Red S staining (Fig. 3D and E) in VSMCs compared with Veh-ECs-CM. Accordingly, the expression of senescence marker P21 (Fig. 3A) and the percentage of  $\beta$ -Gal positive cells (Fig. 3D and F) were also reduced in VSMCs when treated with MT-ECs-CM. However, both depletion of exosomes and inhibition of exosomes secretion in MT-ECs-CM abolished the inhibition effects on VSMCs calcification and senescence, which indicated that it might be exosomes derived from ECs-CM that contribute to MT induced antagonism effects on VSMC calcification and senescence.

To investigate the effects of exosomes derived from MT-ECs-CM on VSMC calcification and senescence, VSMCs were incubated with exosomes isolated from MT-ECs-CM (MT-ECs-Exos) and vehicle-treated ECs CM (Veh-ECs-Exos). Treatment with MT-ECs-Exos significantly reduced Runx2 expression (Fig. 3G), ALP activity (Fig. 3H), calcium content (Fig. 3I) and level of Alizarin Red S staining (Fig. 3J) in VSMCs compared to treatment with Veh-ECs-Exos. Moreover, P21 expression (Fig. 3G) and SA- $\beta$ -Gal staining (Fig. 3J) level were also remarkably

decreased. Fig. 3K and L presents the quantitative analysis results of Alizarin Red S staining and SA- $\beta$ -Gal staining, respectively. These data suggested that exosomes derived from MT-treated ECs suppressed VSMC calcification and senescence.

#### 3.4. MT-induced exosomal miR-302d-5p antagonized VSMC calcification and senescence

MiRNAs are selectively capsulated into exosomes, where they have been reported to be responsible for multiple physiological and pathological processes [36–38]. To examine the role of miRNAs within MT-ECs-Exos in the anti-calcification and anti-senescence effects on VSMCs, we silenced Dicer, an essential enzyme for miRNAs maturation, in ECs to deplete miRNA production. Intriguingly, downregulation of miRNAs in MT-ECs-Exos had negligible effects on ALP activity, expression of Runx2, BMP2, P21, calcium content as well as SA- $\beta$ -gal and Alizarin Red S staining level in recipient VSMCs (Fig. 4A–D), suggesting that exosomal miRNAs play a role in mediating the effects of EC-Exos on VSMCs calcification and senescence. To further clearly determine the underline mechanism involved, we conducted microarray analysis to identify differentially expression miRNAs between MT-ECs-Exos and Veh-ECs-Exos. The results showed that 9 miRNAs were upregulated over two folds while 20 miRNAs were downregulated over two folds in



(caption on next page)

**Fig. 3.** Exosomes derived from MT-treated ECs were responsible for the anti-calcification and anti-senescence effects of melatonin. (A–F) VSMCs were cultured with EC's vehicle-induced CM (Veh-ECs-CM), melatonin-induced CM (MT-ECs-CM), and EVs-depleted MT-CM (MT-ECs-Exo free-CM), and GW4869 pretreated MT-CM (MT-ECs-GW4869-CM). (A) The expression of Runx2, BMP2, P21 of VSMCs was determined by Western blot. (B) The ALP activity in VSMCs was measured by an ALP kit. (C) The calcium content in VSMCs was measured by the o-cresolphthalein method. (D) The calcium nodules in VSMCs was measured by Alizarin red S staining (upper panel, scale bar = 200  $\mu$ m), and the senescence VSMCs was measured by SA- $\beta$ -Gal staining (lower panel, scale bar = 200  $\mu$ m). (E) The quantification results of mineralized nodules staining in figure D. (F) The quantification results of senescence VSMCs in figure D. (G) The expression of Runx2, BMP2, P21 of VSMCs incubated with Veh-ECs-Exos and MT-ECs-Exos was determined by Western blot. (H) The ALP activity in VSMCs incubated with Veh-ECs-Exos or MT-ECs-Exos was measured by an ALP kit. (I) The calcium content in VSMCs treated with Veh-ECs-Exos or MT-ECs-Exos was measured by the o-cresolphthalein method. (J) The calcium nodules in VSMCs treated with Veh-ECs-Exos or MT-ECs-Exos was measured by Alizarin red S staining (upper panel, scale bar = 200  $\mu$ m), the senescence VSMCs was measured by SA- $\beta$ -Gal staining (lower panel, scale bar = 200  $\mu$ m). (K) The quantification results of mineralized nodules staining in figure J. (L) The quantification results of senescence VSMCs in figure J. Three independent experiments were performed, and representative images were shown. Data are shown as mean  $\pm$  SEM. Statistical analysis was performed by one-way ANOVA with Tukey's multiple-comparison test (B-F) and unpaired two-tailed Student's *t*-test (H-L). ns: no significance, \**p* < 0.05, \*\**p* < 0.01.

MT-ECs-Exos compared to Veh-ECs-Exos (Fig. 4E). We further investigated five miRNAs that were significantly upregulated in MT-ECs-Exos, with miR-302d-5p showing the most pronounced difference and hence chosen for further investigation (Fig. 4F). Subsequently, we examined the expression of miR-302d-5p in the medium of MT-ECs, with or without pretreatment with GW4869. Notably, inhibition of exosomes secretion by GW4869 significantly reduced the expression of miR-302d-5p in the medium of MT-treated ECs (Supplemental Figure IV), indicating that miR-302d-5p was encapsulated in MT-ECs-Exos. In addition, miR-302d-5p expression was significantly higher in ECs compared to VSMCs (Supplemental Figure V), and treatment of MT-ECs-Exos increased miR-302d-5p expression in VSMCs compared to treatment with Veh-ECs-Exos (Fig. 4G). To obtain miR-302d-5p over-expressed and down-expressed Exos, ECs were treated with miR-302d-5p mimic or inhibitor, and exosomes were subsequently isolated. Successful knock-in and knockdown of exosomal miR-302d-5p were confirmed (Fig. 4H). Interestingly, PKH26 labeled exosomes (red fluorescent) isolated from ECs transfected with FAM-miR-302d-5p (green fluorescence) exhibited colocalized fluorescence staining when coculture with VSMCs (Fig. 4I), indicating that ECs secreted exosomes containing miR-302d-5p that were transferred into VSMCs. Moreover, knockdown of exosomal miR-302d-5p abolished the inhibitory effects of MT-ECs-Exos on VSMC calcification and senescence, as evidenced by increased ALP activity, higher expression of Runx2 and P21 as well as elevated Alizarin Red S and SA- $\beta$ -gal staining level in recipient VSMCs (Fig. 4J–M). Conversely, re-expression of miR-302d-5p in exosomes derived from miRNAs knock-down ECs significantly restored the anti-calcification and anti-senescence roles of MT-ECs-Exos (Fig. 4N–Q). These findings suggested that exosomal miR-302d-5p played a crucial role in mediating the ability of MT-treated ECs to attenuate VSMC calcification and senescence.

### 3.5. miR-302d-5p inhibited VSMC calcification and senescence by targeting Wnt3

Considering the crucial role of miR-302d-5p in mediating anti-calcification and anti-senescence effects of MT-ECs-Exos, we explored the effects and detailed mechanisms by which miR-302d-5p affected VSMC calcification and senescence. miRNAs exhibit their biological role by binding to the 3' UTR region of target mRNA, and thereby blocking their translation or inducing mRNA degradation. Using bioinformatic target prediction algorithm TargetScan, miRwalk and miRDB, we found 93 overlapping target genes (Fig. 5A). Then we conducted the Gene Ontology (GO) and Kyoto Encyclopedia of Genes and Genomes (KEGG) to analyze the functional enrichment of overlapping target genes. The GO and KEGG analyses indicated that the predicted target genes were enriched in Wnt signalling pathway (Fig. 5B and C). Therefore, we hypothesized that Wnt3 could be the potential target of miR-302d-5p (Fig. 5D). To verify the hypothesis, we constructed luciferase reporter system based on 3'-UTR of Wnt3 containing wild-type or mutated predicted binding sites with miR-302d-5p (WT-pmirGLO-Wnt3 and MUT-pmirGLO-Wnt3, respectively). These constructs and miR-302d-5p

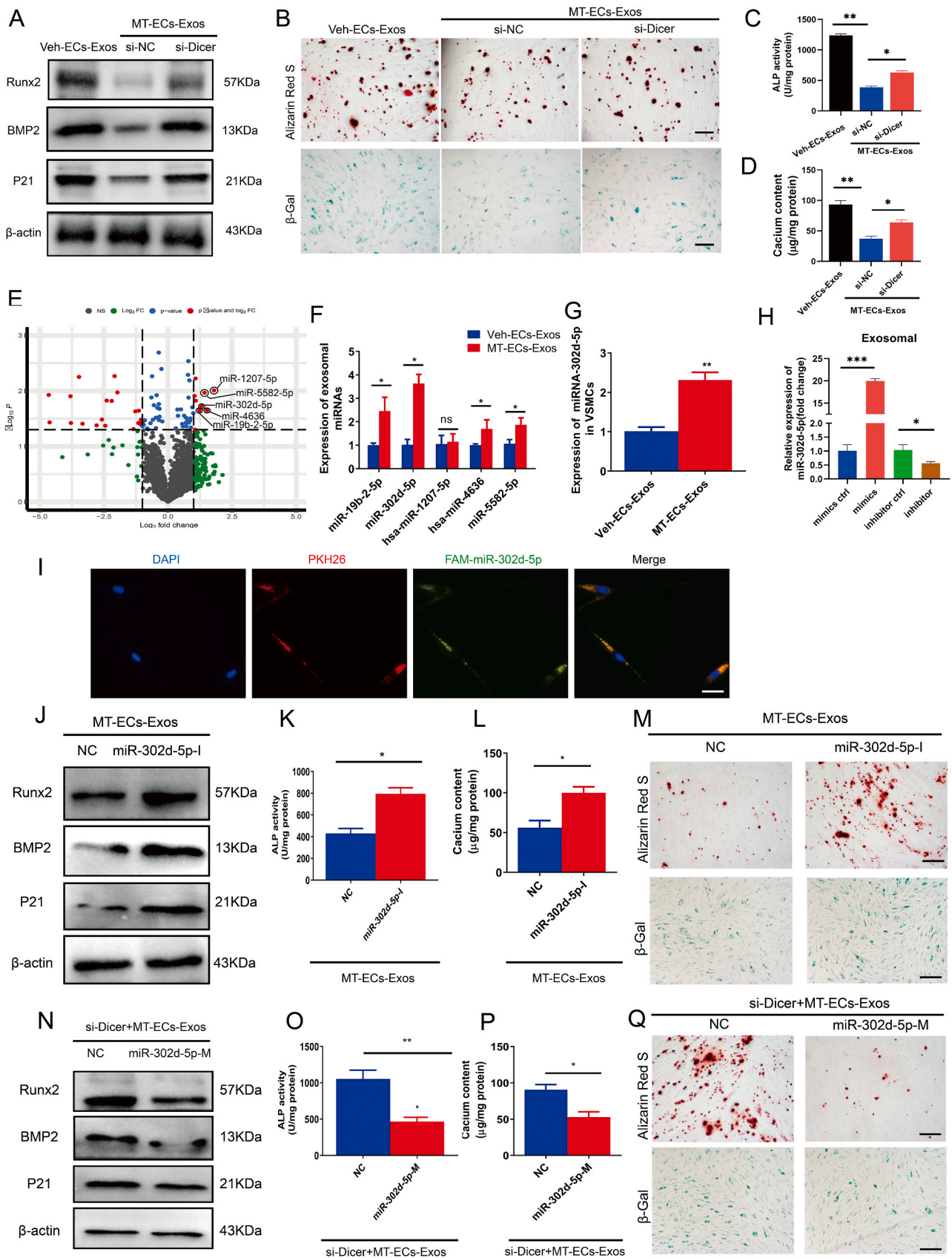
mimics were co-transfected into HEK293T cells, and luciferase activity was subsequently assessed. Overexpression of miR-302d-5p reduced luciferase activity of WT-pmirGLO-Wnt3 compared to control oligos. Conversely, these effects were absent in co-transfection group with miR-302d-5p mimics and MUT-pmirGLO-Wnt3 (Fig. 5E). Furthermore, overexpression of miR-302d-5p significantly suppressed Runx2, BMP2 and P21 expression levels. Conversely, opposite results were obtained when miR-302d-5p was knocked down (Fig. 5F), suggesting miR-302d-5p suppressed VSMCs calcification and senescence. Notably, overexpression of miR-302d-5p antagonist, while downregulation of miR-302d-5p, enhanced the endogenous expression of Wnt3 in VSMCs (Fig. 5F). These data indicated that miR-302d-5p suppressed VSMCs calcification and senescence and negatively regulated Wnt3.

Wnt3, a crucial member of the Wnt family, plays a role in bone formation, a biological process highly resembling VSMCs calcification. Herein, we sought to identify whether Wnt3 was associated with VSMCs calcification and senescence. Transfection of Wnt3 siRNA decreased VSMC calcification and senescence (Fig. 5G–J). Notably, overexpression of Wnt3 blocked anti-calcification and anti-senescence effect of MT-ECs-Exos (Fig. 5K–N). Taken together, these data suggested that Wnt3 contributed to VSMCs calcification and senescence and was the key target of ECs derived exosomal miR-302d-5p.

### 3.6. MT suppressed VSMCs calcification and senescence by inducing the secretion of ECs derived exosomes in a m6A dependent manner

Previous studies have shown that m6A methylation-mediated epigenetic regulation is crucial for the synthesis and degradation of miRNAs [39,40]. In order to explore the upstream molecular mechanism by which melatonin mitigates calcification and senescence, we conducted a bioinformatics analysis on the expression profile of ECs treated with MT (GSE183359). The results showed significant changes in the expression of m6A methylation related writers, erasers and readers, with upregulation of METTL14, WTAP and the demethylase Alkbh5, and downregulation of METTL3, FTO and the RNA-binding proteins eIF3A and YTHDF1 (Fig. 6A). The qRT-PCR verified that WTAP exhibited the most significant difference (Supplemental Figure VI), so WTAP was selected as a candidate functional molecule. We found that following MT incubation, WTAP was significantly up-regulated with a notable decrease in pri-miR-302 expression and an increase in miR-302d-5p expression. However, these alteration of WTAP, pri-miR-302d-5p and mature miR-302d-5p expression were blocked when ECs were pre-treated with the MT receptor inhibitor luzindole (Fig. 6B), suggesting that MT-induced miR-302d-5p processing and maturation in ECs is mediated through WTAP regulation and is MT receptor-dependent.

When ECs were co-cultured with VSMCs under MT induction, the overall m6A methylation level in ECs was significantly increased (Fig. 6C and D). By down-regulating WTAP in ECs, endogenous methylated proteins were immunoprecipitated after UV-crosslinking, and the bound pri-miRNAs were extracted and quantified by qRT-PCR. The results showed a significant reduction in MT-induced methylated pri-miR-302 (Fig. 6E), increased nuclear accumulation of pri-miR-302, and



(caption on next page)

**Fig. 4.** MT-upregulated exosomal miR-302d-5p antagonized VSMC calcification and senescence. (A–D) Dicer, an essential enzyme for miRNAs maturation was silenced in ECs before MT treatment, then Veh-ECs-Exos and MT-ECs-Exos were harvested for VSMCs incubation. (A) The expression levels of Runx2, BMP2, P21 of VSMCs treated by Veh-ECs-Exos or MT-ECs-Exos with or without miRNAs knock-down were detected by Western blot. (B) The calcium nodules in VSMCs treated by Veh-ECs-Exos or MT-ECs-Exos with or without miRNAs knock-down was measured by Alizarin red S staining (upper panel, scale bar = 200  $\mu$ m), the senescence VSMCs were measured by SA- $\beta$ -Gal staining (lower panel, scale bar = 200  $\mu$ m). (C) The ALP activity in VSMCs incubated with Veh-ECs-Exos or MT-ECs-Exos with or without miRNAs knock-down was measured by an ALP kit. (D) The calcium content in VSMCs treated with Veh-ECs-Exos or MT-ECs-Exos with or without miRNAs knock-down was measured by the o-cresolphthalein method. (E) The differentially expressed miRNAs (a cut-off of absolute fold change  $\geq 2.0$  and  $p < 0.05$ ) between Veh-ECs-Exos and MT-ECs-Exos according to microarray analysis. (F) qRT-PCR quantitative results of miRNAs expression levels of Veh-ECs-Exos and MT-ECs-Exos. (G) Expression levels of miR-302d-5p in VSMCs treated with Veh-ECs-Exos and MT-ECs-Exos. (H) Expression levels of miR-302d-5p in exosomes derived from miR-302d-5p over-expressed or down-expressed ECs. (I) Microscopy analysis was used to verify the fluorescent signal colocalization of FAM-miR-302d-5p in green, PKH26 in red and DAPI in blue (scale bar = 50  $\mu$ m). (J) The expression level of Runx2, BMP2, P21 of VSMCs incubated with miR-302d-5p knockdown MT-ECs-Exos was determined by Western blot. (K) The ALP activity in VSMCs incubated with miR-302d-5p knockdown MT-ECs-Exos was measured by an ALP kit. (L) The calcium content in VSMCs treated with miR-302d-5p knockdown MT-ECs-Exos was measured by the o-cresolphthalein method. (M) The calcium nodules in VSMCs treated with miR-302d-5p knockdown MT-ECs-Exos was measured by Alizarin red S staining (upper panel, scale bar = 200  $\mu$ m), the senescence VSMCs was measured by SA- $\beta$ -Gal staining (lower panel, scale bar = 200  $\mu$ m). (N) The expression level of Runx2, BMP2, P21 of VSMCs incubated with miR-302d-5p knock-in Exos was determined by Western blot. (O) The ALP activity in VSMCs incubated with miR-302d-5p knock-in Exos was measured by an ALP kit. (P) The calcium content in VSMCs treated with miR-302d-5p knock-in Exos was measured by the o-cresolphthalein method. (Q) The calcium nodules in VSMCs treated with miR-302d-5p knock-in Exos was measured by Alizarin red S staining (upper panel, scale bar = 200  $\mu$ m), the senescence VSMCs was measured by SA- $\beta$ -Gal staining (lower panel, scale bar = 200  $\mu$ m). Three independent experiments were performed, and representative data were shown. Data were shown as mean  $\pm$  SEM. \* $p < 0.05$ , \*\* $p < 0.01$ , \*\*\* $p < 0.0001$ .

decreased mature miR-302d-5p (Fig. 6F), suggesting that WTAP mediates MT-induced pri-miR-302 m6A methylation. HNRNPA2B1 is known to bind to m6A-methylated pri-miRNA sequences and promote the miRNA processing and maturation [41]. In order to explore whether HNRNPA2B1 acts as reader of the m6A methylation mark in miR-302d-5p processing, endogenous HNRNPA2B1 and interacting partners were immunoprecipitated by specific antibody immobilized with magnetic beads, followed by SDS-PAGE and immunoblotting analysis with the m6A antibody. The co-immunoprecipitation result showed that HNRNPA2B1 interact with the methylated mark (Supplemental Figure VII a). Knocking down HNRNPA2B1 led to the accumulation of pri-miR-302 and reduction of mature miR-302d-5p, similar to the effects of WTAP down-regulation (Fig. 6G). In particular, HNRNPA2B1, a key reading protein in the hnRNP family, has been reported to regulate miRNA processing by interacting with the microprocessor DGCR8 [41]. Immunoprecipitation of endogenous HNRNPA2B1 co-precipitated DGCR8, and reciprocal immunoprecipitation yielded similar results (Supplemental Figure VII b and VII c).

It was found that knocking down WTAP decreased the interaction between DGCR8 and HNRNPA2B1 (Supplemental Figure VII d), while knocking down of HNRNPA2B1 reduced endogenous DGCR8-bound pri-miR-302 (Fig. 6H). Taken together, these results confirm that HNRNPA2B1 recognizes m6A signals created by writer WTAP, then interacted with microprocessor DGCR8 to promote the processing of pri-miR-302. In order to explore whether WTAP mediates the transfer of anti-calcification component from ECs to VSMCs, we knocked down WTAP in ECs, then obtained MT-Exo, and incubated them with VSMCs. The results showed that knocking-down WTAP in ECs attenuated the effect of MT-ECs-Exos on inhibiting VSMC calcification and senescence (Fig. 6I and J). In summary, the above evidences demonstrated that MT-Exo exerted anti-calcification and anti-senescence effects in an m6A-dependent manner.

### 3.7. Exosomes derived from melatonin-treated ECs alleviated vascular calcification and vascular ageing in 5/6 NTP mouse model

To investigate the anti-calcification and anti-ageing effects of MT in 5/6 NTP mice model. MT was administered via gavage for 12 weeks, and the severity of vascular calcification and ageing was evaluated. The results showed that MT significantly ameliorated the severity of vascular calcification and ageing in CKD mice (Supplemental Figure VIII a–g). To elucidate whether MT-ECs-Exos mediate the protective effects against vascular calcification and ageing, MT-ECs-Exos were injected intravenously through tail vein, and their bio-distribution were tracked. Interestingly, DiR-labeled ECs-Exos were mainly distributed in liver, spleen and heart as well as artery tissues (Fig. 7A and B). Quantitative analysis revealed that the intravascular fluorescence signal was stronger

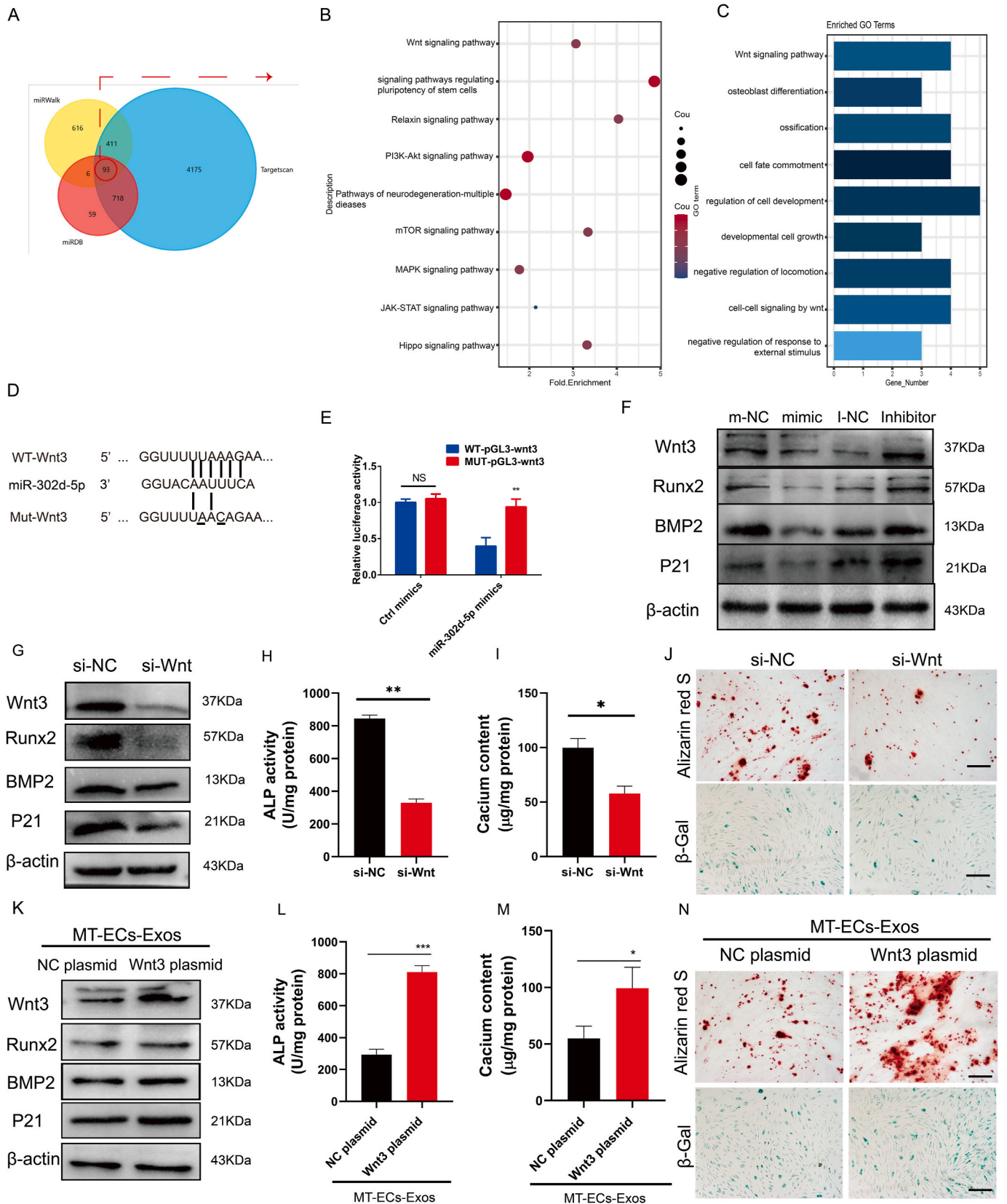
in MT-ECs-Exos than in Veh-ECs-Exos after a single injection, suggesting that MT-ECs-Exos preferentially bind to artery tissues. Worth noting that fluorescent signals persisted after 24 h (Fig. 7C), indicating that exosomes might have the potential for long-term effects. Notably, exosomal marker CD81 exhibited remarkable up-regulation in artery VSMCs from MT-ECs-Exos treated mice compared to Veh-ECs-Exos treated mice, indicating that MT-ECs-Exos are absorbed by aortic VSMCs with higher affinity (Fig. 7D). MT-ECs-Exos infusion markedly decreased the positive area of Alizarin Red S staining, ALP activity and calcium content in the thoracic aorta compared to Veh-ECs-Exos treated mice. This effect was reversed when miR-302d-5p was downregulated in MT-ECs-Exos (Fig. 7E–G). Similarly, the SA- $\beta$ -Gal staining level in thoracic aorta was decreased in MT-ECs-Exos-incubated mice and restored by exosomal miR-302d-5p knockdown (Fig. 7H). Immunohistochemical analysis showed that Runx2 and P21, and Wnt3 expression were consistent with the staining results (Fig. 7I). Taken together, these data showed that MT-ECs-Exos and exosomal miR-302d-5p were absorbed by VSMCs in thoracic aorta tissue, suppressing vascular calcification and vascular ageing.

### 3.8. Endothelial-derived miR-302d-5p attenuated vascular calcification and ageing in CKD mice

To verify the role of endothelial-derived miR-302d-5p in vascular calcification and ageing, we specifically overexpressed miR-302d-5p using the EC-specific promoter (AAV9-TIE-miR-302d-eGFP) via intrasegmental injection into abdominal aorta. Three weeks post-injection, the mice were sacrificed, and the arteries were harvested for analysis (Supplemental Figure IX a). AAV9-TIE-miR-302d-eGFP injection markedly decreased positive area of Alizarin Red S staining (Supplemental Figure IX b), calcium content (Supplemental Figure IX c) and ALP activity (Supplemental Figure VIII e) compared to vector virus-treated mice. Accordingly, SA- $\beta$ -Gal staining level in the thoracic aorta was decreased in endothelial specific miR-302d-5p downregulated mice (Supplemental Figure IX f). Immunohistochemical analysis showed that Runx2, BMP2 as well as P16 and P21 expression were consistent with the staining results (Supplemental Figure IX g and IX h). All these results indicated that overexpression of miR-302d-5p in ECs significantly reduced vascular calcification and ageing in vivo.

## 4. Discussion

In the present study, we have following major novel findings. Firstly, we glean crucial insights into interactions involving exosome-mediated ECs to VSMCs communication triggered by MT in CVD status. Secondly, we provide novel insight into MT-triggered ECs derived exosomes that deliver profound anti-calcification and anti-ageing effects in the



(caption on next page)

**Fig. 5.** miR-302d-5p inhibits VSMCs calcification and senescence by targeting Wnt3 (A) The Venn diagram of target genes of miR-302d-5p predicted by TargetScan, miRwalk and miRDB. (B) Gene Ontology analysis of overlapping target genes of miR-302d-5p. (C) Kyoto Encyclopedia of Genes and Genomes (KEGG) analysis of overlapping target genes of miR-302d-5p. (D) Schematic representation of miR-302d-5p putative target sites in Wnt3 3'-UTR and alignment of miR-302d-5p with WT and MUT Wnt3 3'-UTR showing pairing. (E) Luciferase activity was performed using luciferase constructs carrying a wild type or mutant Wnt3 3'-UTR co-transfected into HEK293T cells with miR-302d-5p mimics compared with empty vector control. (F) The expression level of Wnt3, Runx2, BMP2, P21 in VSMCs treated with miR-302d-5p mimic or inhibitor. (G–J) VSMCs were incubated with Wnt3 silencing by siRNA interference. Then, the expression level of Wnt3, Runx2, P16, P21 (G), ALP activity (H), calcium content (I) and mineralized nodules (J, upper panel, scale bar = 200  $\mu$ m) as well as senescence cells (J, lower panel, scale bar = 200  $\mu$ m) was measured in VSMCs. (K–N) VSMCs were transfected with Wnt3 overexpression plasmid before MT-ECs-Exos incubation. Then, the expression level of Wnt3, Runx2, P16, P21 (K), ALP activity (L), calcium content (M) and mineralized nodules (N, upper panel) as well as senescence cells (N, lower panel) was measured in VSMCs (scale bar = 200  $\mu$ m). Results are represented by mean  $\pm$  SEM for each group. \* $p$  < 0.05. \*\* $p$  < 0.01, \*\*\* $p$  < 0.001.

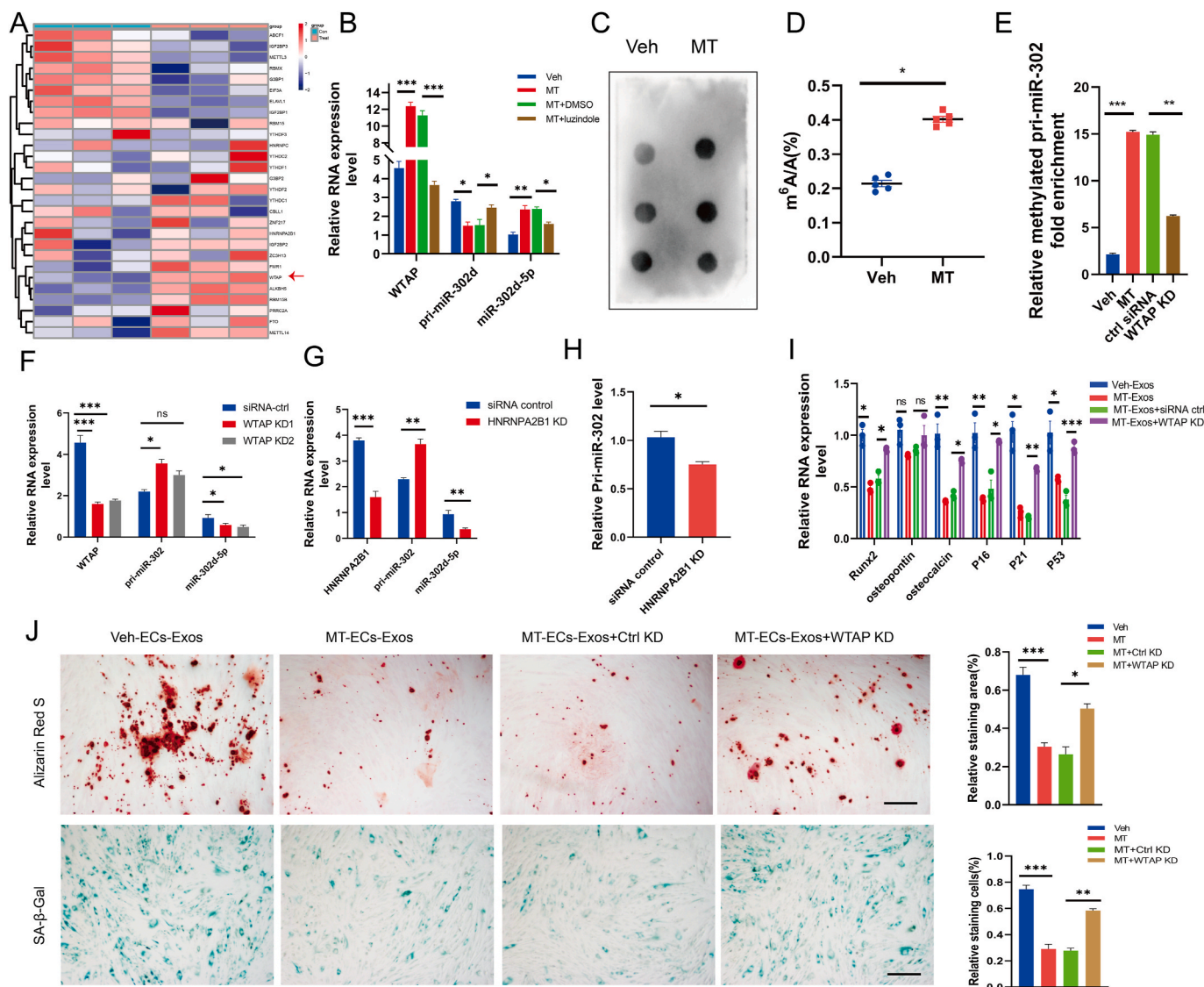


**Fig. 6.** MT suppresses VSMC calcification and aging by inducing ECs derived exosomes secretion in a m6A dependent manner. (A) Expression heatmap of m6A-related genes in ECs before and after MT treatment. (B) qRT-PCR confirmed that the expression level of WTAP, pri-miR-302, miR-302d-5p of ECs treated with Veh, MT, MT plus DMSO, MT plus luzindole respectively. (C) Dot blot identified m6A modification levels of total RNA in ECs undergoing Veh and MT interventions. (D) The m6A content of total RNA from ECs treated with Veh or MT was measured by ELISA using an EpiQuik m6A RNA methylation quantification kit. (E) The expression level of methylated pri-miR-302 was measured by MeRIP-PCR. (F) qRT-PCR confirmed that the expression level of WTAP, pri-miR-302, miR-302d-5p of ECs after knock-down of WTAP. (G) qRT-PCR confirmed that the expression level of HNRNPA2B1, pri-miR-302, miR-302d-5p of ECs after knock-down of HNRNPA2B1. (H) Detection of pri-miR-302 binding to DGCR8 by immunoprecipitation experiments in control and HNRNPA2B1 down-expression ECs. (I) The expression level of Runx2, osteopontin, osteocalcin, P16, P21, P53 in Veh-ECs-Exos, MT-ECs-Exos, MT-ECs-Exos plus siRNA ctrl and MT-ECs-Exos plus WTAP KD treated ECs. (J) The calcium nodules in VSMCs was measured by Alizarin red S staining (upper panel, scale bar = 200  $\mu$ m), the senescence VSMCs was measured by SA- $\beta$ -Gal staining (lower panel, scale bar = 200  $\mu$ m). Results are represented by mean  $\pm$  SEM. \* $p$  < 0.05. \*\* $p$  < 0.01, \*\*\* $p$  < 0.001.

vascular. Thirdly, we identify that MT induced miR-302d-5p maturation and enrichment through HNRNPA2B1/DGCR8 pathway in a m6A dependent manner. Lastly, ECs-derived exosomal miR-302d-5p works as

the predominant molecule that inhibits Wnt3 and alleviates vascular calcification and ageing in the artery of CKD-induced mice. Our present work provides a novel intercellular communication mechanism that

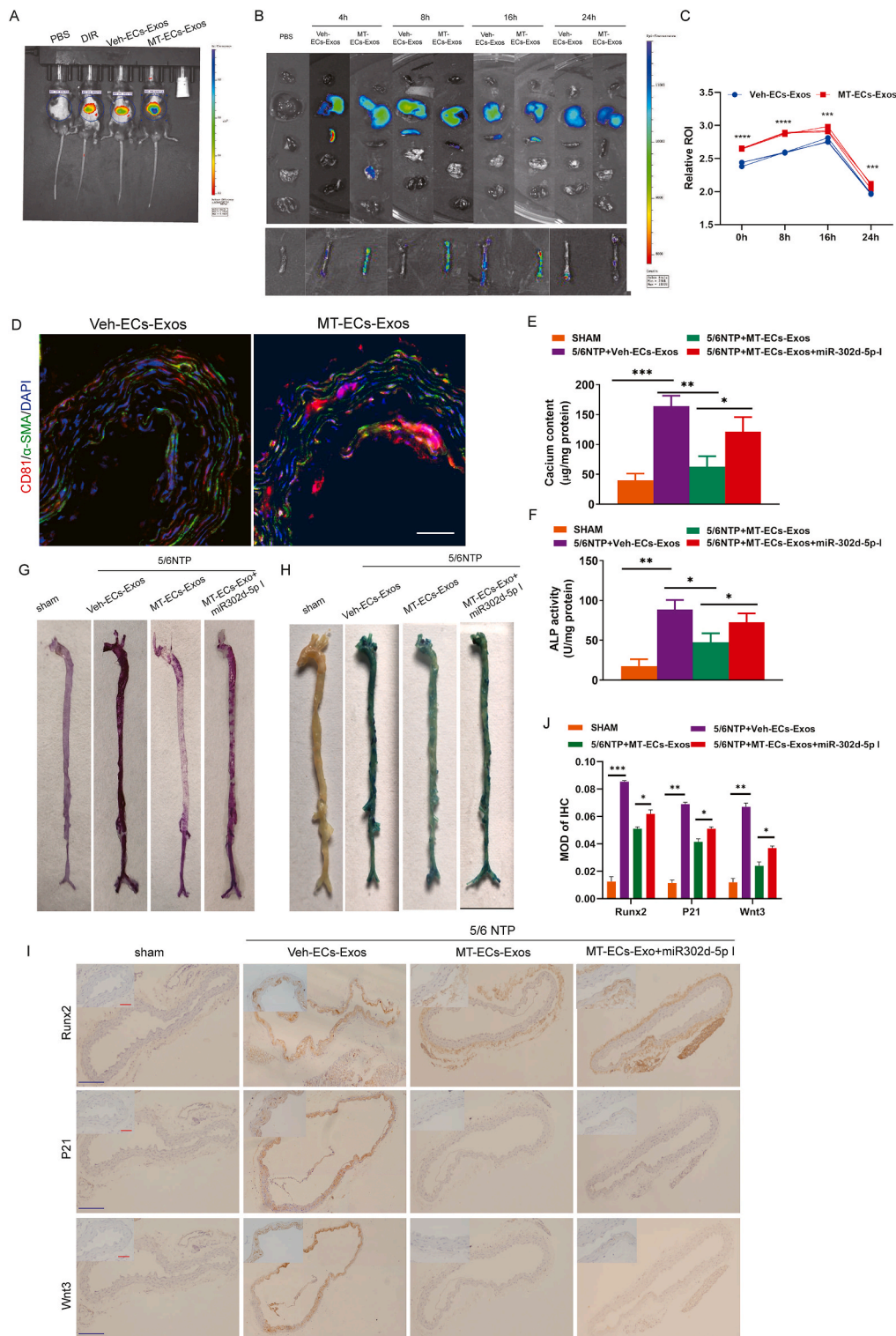


**Fig. 7.** Exosomes derived from melatonin-treated ECs alleviated vascular calcification and vascular aging in 5/6 NTP mice model. (A) Spectrum in vivo imaging results of mice injected with PBS, fluorescent dye DIR, and DIR-labeled exosome via tail vein, respectively (n = 6). (B) Spectrum imaging results of organs harvested from mice injected intravenously with PBS, and DIR-labeled exosome for 4h, 8h, 16h, 24h, respectively (n = 6). (C) Quantitation of relative fluorescent ROI between organs from Veh-ECs-Exos and MT-Exo infused mice at 0h, 8h, 16h, 24h (n = 6). (D) The thoracic aorta was obtained to analyze the uptake of endothelial exosomes in the slices after injection 24h. Blue fluorescence (DAPI)-labeled cell nuclei, green fluorescence (Alexa 488)-labeled  $\alpha$ -SMA, and red fluorescence (Alexa 555)-labeled CD81 indicating exosomes (n = 6, scale bar = 50  $\mu$ m). (E–H) Veh-ECs-Exos, MT-ECs-Exos, and MT-ECs-Exos transfected with miR-302d-5p inhibitor (MT-ECs-Exos + miR-302d-5p-I) were injected to 5/6 NTP mice. (E) Calcium content of thoracic aorta of mice was measured by o-cresolphthalein method. (F) The ALP activity level among four groups measured by ALP kit (n = 6). (G) thoracic aorta calcification was analyzed by Alizarin Red S staining (n = 6). (H) SA- $\beta$ -gal-stained micrographs were presented to reveal aorta senescence (n = 6). (I) Immunohistochemistry analysis of Runx2, P21 and Wnt3 in thoracic aorta (n = 5). Scale bar 50  $\mu$ m (Red) and 500  $\mu$ m (Blue). (J) Quantitation of middle OD of IHC. Results were represented by mean  $\pm$  SEM. \* $p$  < 0.05, \*\* $p$  < 0.01, \*\*\* $p$  < 0.001, \*\*\*\* $p$  < 0.0001.

maintains vascular homeostasis and protects against the progression of CVD.

Single-cell RNA sequencing revealed cell type and artery type-specific vascular remodeling. The transcriptional landscape exhibited heterogeneity of aortic cells in human with vascular diseases. Especially ECs, beyond serving as the natural barrier of vascular against exogenous stimulation and artery flow, have now been demonstrated to modulate VSMCs phenotypes and functions<sup>24,25</sup>. Recent studies have highlighted that dysfunction ECs secrete multiple factors, such as forkhead box M1, which affect VSMCs proliferation and apoptosis as well as phenotype switching [42]. However, whether ECs carrying exosomes affect VSMCs functions remains largely unknown. Recently, Boyer et al. reported that ECs-derived exosomes stimulated protein synthesis and senescence in VSMCs [43]. Under high glucose stimulation, ECs secreted exosomes containing proteins such as Notch3 and versican, which could enhance VSMCs calcification and senescence [44,45]. In our present study, MT-stimulated ECs secreted anti-calcifying and anti-ageing exosomes, highlighting their potential in ameliorating vascular calcification and vascular ageing. The above findings add new insights to our previous studies that MT alleviated vascular calcification and vascular ageing by inducing exosomes mediating crosstalk across the artery wall [21]. Besides, our findings provide further evidence that ECs are candidate targets to prevent the progression of medial vascular diseases. However, because of rapid clearance by the macrophage and biological barriers, using exosomes for therapeutic purposes to achieve the target cells is of greater importance and is also a major challenge up to now. Notably, we found endothelial derived MT-ECs-Exos maintained a longer half-life in serum and greater accumulation in targeting artery tissues, suggesting stronger biological activity of MT-ECs-Exos. We proposed that the increased stability of exosomes might be associated with higher expression of CD47, a key membrane protein that signals “do not eat me” to immune cells, resulting in reduced phagocytosis by macrophages [46]. However, we did not verify this hypothesis by examining the expression of CD47. Further studies are needed to verify the detailed mechanism. Taken together, these data identify that MT treatment improves not only the quality but also the stability of exosomes, thereby exerting profound cardioprotective bioactivity.

Recent studies have highlighted that exosomal miRNAs are selectively encapsulated into exosomes to induce profound bioactivity in the recipient cells [47]. For instance, adipose-specific depletion of miRNAs markedly reduces circulating exosomal miRNAs expression, resulting in higher expression of FGF21, an important target of exosomal miRNAs, in other tissues [48]. Additionally, miR-690 is selectively encapsulated into M2-macrophage-driven exosomes, improving on insulin sensitivity in various recipient tissues such as liver and skeletal muscle [38]. Our previous studies have identified the miRNAs profiles in MT-treated VSMCs and demonstrate the critical roles of miR-204/221 clusters [21]. Herein, we reported that miR-302d-5p, which was nearly absent in VSMCs, is specifically enriched in exosomes derived from MT-induced ECs, resulting in higher expression of miR-302d-5p in recipient VSMCs both *in vitro* and *in vivo*. To verify that miR-302d-5p contributes to exosomes induced alleviation of vascular calcification and vascular ageing, miR-302d-5p is encapsulated into miRNAs knock-down ECs-derived exosomes. Intriguingly, the inhibition effects of MT-ECs-Exosomes on vascular calcification and vascular ageing were remarkably rescued by re-expression of miR-302d-5p in EC-exosomes, which highly resembling the effects of MT-ECs-Exos. Taken together, these data favor our hypothesis that ECs transfer miR-302d-5p to VSMCs to attenuate vascular calcification and vascular ageing under MT induction. Additionally, these data identify the critical roles of exosomal miR-302d-5p in the calcification and ageing of arterial tissues.

Another important finding of our present work is the identification of the miR-302d-5p/Wnt3 axis in the regulation of vascular calcification and vascular ageing. Little has been investigated regarding the roles of miR-302d-5p, except for its role in favoring cardiomyocyte proliferation [49]. Indeed, we found that miR-302d-5p exhibited significant

inhibitory effects on VSMCs calcification and ageing. Furthermore, using bioinformatic analysis and luciferase reporter gene system, we demonstrated that Wnt3 is a bona fide target mRNA of miR-302d-5p. However, further studies are needed to elucidate the role of Wnt3 in the progression of vascular calcification and vascular ageing.

N6-methyladenosine (m6A) is the most abundant and reversible internal mRNA modification, which is catalyzed by the methyltransferase complex, including METTL3, METTL14, and WTAP, and reversed by demethylase FTO and ALKBH5 [50–52]. The m6A modification has been revealed to affect the splicing, exportation, localization, translation, and stability of target mRNAs, thereby proved to functioning in a variety of cardiovascular diseases such as myocardial hypertrophy, myocardial infarction, hypertension, etc [53–57]. However, little has been reported for the role of WTAP in vascular calcification and ageing. In the present study, we found that maturation of endothelial derived exosomal miR-302d-5p was promoted by WTAP in an m6A-dependent manner. Importantly, among the differential expressed gene associated with m6A regulation, WTAP was marked promoted by MT. Our findings drive new insight of m6A dependent regulation of potent miRNAs, such as miR-302d-5p, in response to MT stimulation.

Surprisingly, we found that in NTP mice, MT-ECs-Exos injection for 1 month could attenuate vascular calcification and ageing. At the same time, when exosomal miR-302d-5p was inhibited, the anti-calcification and anti-ageing effect of MT-ECs-Exos was greatly weakened. These results indicated the superiority of exosomes as a therapeutic carrier and their application potential of transforming therapeutic cargos.

The present study has some limitations. Firstly, we could only control the expression of miR-302d-5p in exosomes by using miR-302d-5p mimics or inhibitor. Further studies are needed to establish miR-302d-5p conditional knockout mice to verify the role of EC-derived miR-302d-5p in the progression of vascular calcification and vascular ageing. Secondly, animal studies are needed to verify the roles of miR-302d-5p and Wnt3 in the progression of vascular calcification and vascular ageing. Finally, it is possible that additional exosomal proteins or RNAs contribute to the bioactivity of MT.

Altogether, our finding revealed the potential role of MT from aortic transcriptional landscape. Eventually, we discovered that MT-ECs-Exos alleviated vascular calcification and vascular ageing through miR-302d-5p/Wnt3 signaling pathway in an m6A dependent way. Our research, based on the microenvironment of vascular wall, revealed both upstream and downstream mechanism of MT in restoring vascular homeostasis and health through the information transportation between ECs and VSMCs. It will help broaden the understanding of pivotal role of multi-cellular interaction in pathological vascular calcification and ageing, and provided a solid research basis for the development of novel therapeutic targets.

#### Declaration of competing interest

The authors declare that they have no known competing financial interests or personal relationships that could have appeared to influence the work reported in this paper.

#### Funding

This work was supported by National Key Research & Development Program (No.2021YFC2501701 to LQY and FX), the National Natural Science Foundation of China (No.82370892 and 82070910 to LQY; No.82100494 to FX; No.82100944 and No.82470927 to XL; No.82200869 to FW), National Clinical Key Specialties Main Research Projects (2023026 to LQY), the Natural Science Foundation of Hunan Province (No.2022JJ40721 to FX), the Health Research Project in Hunan Province (No.20231696 to XL), and the Scientific Research Launch Project for new employees of the Second Xiangya Hospital of Central South University (No.7673 to FX).

## CRedit authorship contribution statement

**Su-Kang Shan:** Writing – review & editing, Writing – original draft, Visualization, Validation, Supervision, Resources, Project administration, Methodology. **Xiao Lin:** Funding acquisition, Data curation. **Feng Wu:** Funding acquisition, Data curation. **Chang-Chun Li:** Writing – original draft, Software. **Bei Guo:** Methodology, Formal analysis. **Fu-Xing-Zi Li:** Resources, Conceptualization. **Ming-Hui Zheng:** Software, Resources, Conceptualization. **Yi Wang:** Software, Resources. **Qiu-Shuang Xu:** Software, Resources. **Li-Min Lei:** Visualization, Validation. **Ke-Xin Tang:** Project administration, Methodology. **Yun-Yun Wu:** Visualization, Validation. **Jia-Yue Duan:** Visualization, Validation. **Ye-Chi Cao:** Visualization, Validation. **Yan-Lin Wu:** Writing – review & editing. **Chang-Ming Tan:** Supervision. **Zi-Han Liu:** Data curation. **Zhi-Ang Zhou:** Validation, Methodology. **Xiao-Bo Liao:** Investigation, Funding acquisition. **Feng Xu:** Writing – review & editing, Writing – original draft, Investigation, Funding acquisition, Data curation. **Ling-Qing Yuan:** Writing – review & editing, Supervision, Funding acquisition, Data curation, Conceptualization.

## Appendix A. Supplementary data

Supplementary data to this article can be found online at <https://doi.org/10.1016/j.bioactmat.2024.08.021>.

## References

- C. Onnis, R. Virmani, K. Kawai, et al., Coronary artery calcification: current concepts and clinical implications, *Circulation* 149 (3) (2024) 251–266.
- P. Lanzer, F.M. Hannan, J.D. Lanzer, et al., Medial arterial calcification: JACC state-of-the-art review, *J. Am. Coll. Cardiol.* 78 (11) (2021) 1145–1165.
- Y.Y. Wu, S.K. Shan, X. Lin, et al., Cellular crosstalk in the vascular wall microenvironment: the role of exosomes in vascular calcification, *Front Cardiovasc Med* 9 (2022) 912358.
- N.A. Rashdan, A.M. Sim, L. Cui, et al., Osteocalcin regulates arterial calcification via altered Wnt signaling and glucose metabolism, *J. Bone Miner. Res. : the official journal of the American Society for Bone and Mineral Research* 35 (2) (2020) 357–367.
- C. Wang, W. Xu, J. An, et al., Poly(ADP-ribose) polymerase 1 accelerates vascular calcification by upregulating Runx2, *Nat. Commun.* 10 (1) (2019) 1203.
- F. Yang, Q. Chen, S. He, et al., miR-22 is a novel mediator of vascular smooth muscle cell phenotypic modulation and neointima formation, *Circulation* 137 (17) (2018) 1824–1841.
- X. Lin, F. Xu, R.-R. Cui, et al., Arterial calcification is regulated via an miR-204/DNMT3a regulatory circuit both in vitro and in female mice, *Endocrinology* 159 (8) (2018) 2905–2916.
- J. Wu, L. Kuang, C. Chen, et al., miR-100-5p-abundant exosomes derived from infrapatellar fat pad MSCs protect articular cartilage and ameliorate gait abnormalities via inhibition of mTOR in osteoarthritis, *Biomaterials* 206 (2019) 87–100.
- F. Xu, F.-X.-Z. Li, X. Lin, et al., Adipose tissue-derived omentin-1 attenuates arterial calcification via AMPK/Akt signaling pathway, *Aging* 11 (20) (2019) 8760–8776.
- L.-M. Yu, X. Dong, X.-D. Xue, et al., Melatonin attenuates diabetic cardiomyopathy and reduces myocardial vulnerability to ischemia-reperfusion injury by improving mitochondrial quality control: role of SIRT6, *J. Pineal Res.* 70 (1) (2021) e12698.
- J. Zhang, X. Lu, M. Liu, et al., Melatonin inhibits inflammasome-associated activation of endothelium and macrophages attenuating pulmonary arterial hypertension, *Cardiovasc. Res.* 116 (13) (2020) 2156–2169.
- R. Isaac, F.C.G. Reis, W. Ying, J.M. Olefsky, Exosomes as mediators of intercellular crosstalk in metabolism, *Cell Metabol.* 33 (9) (2021) 1744–1762.
- S. Sahoo, M. Adamiak, P. Mathiyalagan, F. Kenneweg, S. Kafert-Kasting, T. Thum, Therapeutic and diagnostic translation of extracellular vesicles in cardiovascular diseases: roadmap to the clinic, *Circulation* 143 (14) (2021) 1426–1449.
- K. Qiao, X. Cui, J. Gao, et al., Roles of extracellular vesicles derived from immune cells in atherosclerosis, *Extracellular Vesicle* 2 (100028) (2023).
- Y. Zhang, W. Wu, X. Pan, et al., Extracellular vesicles as novel therapeutic targets and diagnosis markers, *Extracellular Vesicle* 1 (100017) (2022).
- M. Spanos, P. Gokulnath, E. Chatterjee, et al., Expanding the horizon of EV-RNAs: lncRNAs in EVs as biomarkers for disease pathways, *Extracellular Vesicle* 2 (100025) (2023).
- T.J. Ellison, S.L. Stice, Y. Yao, Therapeutic and diagnostic potential of extracellular vesicles in amyotrophic lateral sclerosis, *Extracellular Vesicle* 2 (100019) (2023).
- K.D. Popowski, D.E. López, B. Juan Abad, A. George, et al., Inhalable exosomes outperform liposomes as mRNA and protein drug carriers to the lung, *Extracellular Vesicle* 1 (100002) (2022).
- M.J. Boyer, Y. Kimura, T. Akiyama, et al., Endothelial cell-derived extracellular vesicles alter vascular smooth muscle cell phenotype through high-mobility group box proteins, *J. Extracell. Vesicles* 9 (1) (2020) 1781427.
- B. Zheng, W.N. Yin, T. Suzuki, et al., Exosome-mediated miR-155 transfer from smooth muscle cells to endothelial cells induces endothelial injury and promotes atherosclerosis, *Mol. Ther.* 25 (6) (2017) 1279–1294.
- F. Xu, J.Y. Zhong, X. Lin, et al., Melatonin alleviates vascular calcification and ageing through exosomal miR-204/miR-211 cluster in a paracrine manner, *J. Pineal Res.* 68 (3) (2020) e12631.
- X. Lin, T. Zhu, F. Xu, J.Y. Zhong, F. Li, S.K. Shan, F. Wu, B. Guo, M.H. Zheng, Y. Wang, Q.S. Xu, X.B. Liao, H.Y. Lu, X.B. Xie, L.Q. Yuan, Plasma exosomes derived from patients with end-stage renal disease and renal transplant recipients have different effects on vascular calcification, *Front. Cell Dev. Biol.* 28 (8) (2021) 618228.
- F. Xu, J.Y. Zhong, B. Guo, X. Lin, F. Wu, F.X. Li, S.K. Shan, M.H. Zheng, Y. Wang, Q. S. Xu, L.M. Lei, C.M. Tan, X.B. Liao, L.Q. Yuan, H19 promotes osteoblastic transition by acting as ceRNA of miR-140-5p in vascular smooth muscle cells, *Front. Cell Dev. Biol.* 7 (10) (2022) 774363.
- X. Lin, S.-K. Shan, F. Xu, et al., The crosstalk between endothelial cells and vascular smooth muscle cells aggravates high phosphorus-induced arterial calcification, *Cell Death Dis.* 13 (7) (2022) 650.
- B. Guo, S.-K. Shan, F. Xu, et al., Protective role of small extracellular vesicles derived from HUVECs treated with AGEs in diabetic vascular calcification, *J Nanobiotechnology* 20 (1) (2022) 334.
- M.-H. Zheng, S.-K. Shan, X. Lin, et al., Vascular wall microenvironment: exosomes secreted by adventitial fibroblasts induced vascular calcification, *J Nanobiotechnology* 21 (1) (2023) 315.
- Y. Hu, A.H. Baker, Y. Zou, A.C. Newby, Q. Xu, Local gene transfer of tissue inhibitor of metalloproteinase-2 influences vein graft remodeling in a mouse model, *Arterioscler. Thromb. Vasc. Biol.* 21 (8) (2001) 1275–1280.
- T. Ali, H. Badshah, T.H. Kim, M.O. Kim, Melatonin attenuates D-galactose-induced memory impairment, neuroinflammation and neurodegeneration via RAGE/NF-κB/JNK signaling pathway in aging mouse model, *J. Pineal Res.* 58 (1) (2015) 71–85.
- F.-X.-Z. Li, J.-J. Liu, F. Xu, et al., Cold exposure protects against medial arterial calcification development via autophagy, *J Nanobiotechnology* 21 (1) (2023) 226.
- B.R. Lindman, J. Lindenfeld, Prevention and mitigation of heart failure in the treatment of calcific aortic stenosis: a unifying therapeutic principle, *JAMA Cardiol* 6 (9) (2021) 993–994.
- B. Simonson, M. Chaffin, M.C. Hill, et al., Single-nucleus RNA sequencing in ischemic cardiomyopathy reveals common transcriptional profile underlying end-stage heart failure, *Cell Rep.* 42 (2) (2023) 112086.
- E.L. Chou, M. Chaffin, B. Simonson, et al., Aortic cellular diversity and quantitative genome-wide association study trait prioritization through single-nuclear RNA sequencing of the aneurysmal human aorta, *Arterioscler. Thromb. Vasc. Biol.* 42 (11) (2022) 13551374.
- S.K. Mohanta, L. Peng, Y. Li, et al., Neuroimmune cardiovascular interfaces control atherosclerosis, *Nature* 605 (7908) (2022) 152–159.
- F. Rutsch, I. Buers, Y. Nitschke, Hereditary disorders of cardiovascular calcification, *Arterioscler. Thromb. Vasc. Biol.* 41 (1) (2021) 35–47.
- G. Santulli, A. Wronska, K. Uryu, et al., A selective microRNA-based strategy inhibits restenosis while preserving endothelial function, *J. Clin. Invest.* 124 (9) (2014) 4102–4114.
- W. Ying, M. Riopel, G. Bandyopadhyay, et al., Adipose tissue macrophage-derived exosomal miRNAs can modulate in vivo and in vitro insulin sensitivity, *Cell* 171 (2) (2017) 372–384. e12.
- R. Garcia-Martin, G. Wang, B.B. Brandão, et al., MicroRNA sequence codes for small extracellular vesicle release and cellular retention, *Nature* 601 (7893) (2022) 446–451.
- W. Ying, H. Gao, F.C.G. Dos Reis, et al., MiR-690, an exosomal-derived miRNA from M2-polarized macrophages, improves insulin sensitivity in obese mice, *Cell Metab.* 33 (4) (2021) 781–790.e5.
- Y.L. Wu, Z.J. Lin, C.C. Li, et al., Epigenetic regulation in metabolic diseases: mechanisms and advances in clinical study, *Signal Transduct. Targeted Ther.* 8 (1) (2023) 98.
- F. Fabbiano, J. Corsi, E. Gurrieri, C. Trevisan, M. Notarangelo, V.G. D'Agostino, RNA packaging into extracellular vesicles: an orchestra of RNA-binding proteins? *J Nanobiotechnology* 10 (2) (2020) e12043.
- C.R. Alarcón, H. Goodarzi, H. Lee, X. Liu, S. Tavazoie, S.F. Tavazoie, HNRNPA2B1 is a mediator of m(6)a-dependent nuclear RNA processing events, *Cell* 162 (6) (2015) 1299–1308.
- M. Balcells, J. Martorell, C. Olivé, et al., Smooth muscle cells orchestrate the endothelial cell response to flow and injury, *Circulation* 121 (20) (2010) 2192–2199.
- M.J. Boyer, Y. Kimura, T. Akiyama, et al., Endothelial cell-derived extracellular vesicles alter vascular smooth muscle cell phenotype through high-mobility group box proteins, *J. Extracell. Vesicles* 9 (1) (2020) 1781427.
- S. Li, J.-K. Zhan, Y.-J. Wang, et al., Exosomes from hyperglycemia-stimulated vascular endothelial cells contain versican that regulate calcification/senescence in vascular smooth muscle cells, *Cell Biosci.* 9 (2019) 1.
- X. Lin, S. Li, Y.-J. Wang, et al., Exosomal Notch3 from high glucose-stimulated endothelial cells regulates vascular smooth muscle cells calcification/aging, *Life Sci.* 232 (2019) 116582.
- S. Kamerkar, V.S. LeBleu, H. Sugimoto, et al., Exosomes facilitate therapeutic targeting of oncogenic KRAS in pancreatic cancer, *Nature* 546 (7659) (2017) 498–503.
- Z. Wei, A.O. Batagov, S. Schinelli, et al., Coding and noncoding landscape of extracellular RNA released by human glioma stem cells, *Nat. Commun.* 8 (1) (2017) 1145.

- [48] T. Thomou, M.A. Mori, J.M. Dreyfuss, et al., Adipose-derived circulating miRNAs regulate gene expression in other tissues, *Nature* 542 (7642) (2017) 450–455.
- [49] F. Xu, J. Yang, J. Shang, et al., MicroRNA-302d promotes the proliferation of human pluripotent stem cell-derived cardiomyocytes by inhibiting in the Hippo pathway, *Clin Sci (Lond)*. 133 (13) (2019) 1387–1399.
- [50] I.A. Roundtree, M.E. Evans, T. Pan, C. He, Dynamic RNA modifications in gene expression regulation, *Cell* 169 (7) (2017) 1187–1200.
- [51] J. Liu, X. Dou, C. Chen, et al., N6-methyladenosine of chromosome-associated regulatory RNA regulates chromatin state and transcription, *Science* 367 (6477) (2020) 580–586.
- [52] J. Wei, X. Yu, L. Yang, X. Liu, C. He, FTO mediates LINE1 m6A demethylation and chromatin regulation in mESCs and mouse development, *Science*. 376 (6596) (2022) 968–973.
- [53] L.E. Dorn, L. Lasman, J. Chen, X. Xu, T.J. Hund, M. Medvedovic, J.H. Hanna, J. H. van Berlo, F. Accornero, The N6-methyladenosine mRNA methylase METTL3 controls cardiac homeostasis and hypertrophy, *Circulation* 139 (4) (2019) 533–545.
- [54] X.Q. Gao, Y.H. Zhang, F. Liu, K. Wang, The piRNA CHAPIR regulates cardiac hypertrophy by controlling METTL3-dependent N6-methyladenosine methylation of Parp10 mRNA, *Nat. Cell Biol.* 22 (11) (2020) 1319–1331.
- [55] P. Mathiyalagan, M. Adamiak, J. Mayourian, Y. Sassi, Y. Liang, N. Agarwal, D. Jha, S. Zhang, E. Kohlbrenner, E. Chepurko, J. Chen, M.G. Trivieri, R. Singh, R. Bouchareb, K. Fish, K. Ishikawa, D. Lebeche, R.J. Hajjar, S. Sahoo, FTO-dependent N6-methyladenosine regulates cardiac function during remodeling and repair, *Circulation* 139 (4) (2019) 518–532.
- [56] R. Kumari, P. Ranjan, Z.G. Suleiman, S.K. Goswami, J. Li, R. Prasad, S.K. Verma, mRNA modifications in cardiovascular biology and disease: with a focus on m6A modification, *Cardiovasc. Res.* 118 (7) (2022) 1680–1692.
- [57] L. Hu, Y. Yu, Y. Shen, F. Chen, Ythdf2 promotes pulmonary hypertension by suppressing Hmox1-dependent anti-inflammatory and antioxidant function in alveolar macrophages, *Redox Biol.* 61 (2023) 102638.